# Paragenesis of multiple platinum-group mineral populations in Shetland ophiolite chromitite: 3D X-ray tomography and in situ Os isotopes

H. M. Prichard[a,d], Stephen J. Barnes[b*], C. W. Dale[c], B. Godel [b], and P. C. Fisher[a], G. M. Nowell[c]

[a]*School of Earth and Ocean Sciences, Cardiff University, Cardiff, CF10 3AT, Wales, UK.*

[b]*CSIRO Mineral Resources, Perth, WA, Australia.*

[c]*DGC, Department of Earth Sciences, Durham University, Durham, DH1 3LE, UK.*

[d]*Deceased, Jan 1 2017.*

*steve.barnes@csiro.au corresponding author

*016*

Key words:- PGM, PGE, Chromite, X-ray computed tomography, laurite, Shetland ophiolite.

**Abstract**

Chromitite from the Harold's Grave locality in the mantle section of the Shetland ophiolite complex is extremely enriched in Ru, Os and Ir, at µg/g concentrations. Volumes were collected on micro-cores from these chromitites using high-resolution X-ray computed tomography have been processed to determine the location, size, distribution and morphology of the platinum-group minerals (PGM). There are five generations of PGM in these chromitites. Small (average 5 µm in equivalent sphere diameter, ESD) euhedral laurites, often with Os-Ir alloys, are totally enclosed in the chromite and are likely to have formed first by direct crystallisation from the magma as the chromite crystallised. Also within the chromitite there are clusters of larger (50 µm ESD) aligned elongate crystals of Pt-, Rh-, Ir-, Os- and Ru-bearing PGM that have different orientations in different chromite crystals. These may have formed either by exsolution, or by preferential nucleation of PGMs in boundary layers around particular growing chromite grains. Thirdly there is a generation of large (100µm ESD) composite Os-Ir-Ru-rich PGM that are all interstitial to the chromite grains and sometimes form in clusters. It is proposed that Os, Ir and Ru in this generation were concentrated in base metal sulfide droplets that were then re-dissolved into a later S undersaturated magma, leaving PGM interstitial to the chromite grains. Fourthly there is a group of almost spherical large (80 µm ESD) laurites, hosting minor Os-Ir-Ru-rich PGM that form on the edge or enclosed in chromite grains occurring in a sheet crosscutting a chromitite layer. These may be hosted in an annealed late syn- or post magmatic fracture. Finally a few of the PGM have been deformed in localised shear zones through the chromitites.

The vast majority of the PGM – including small PGM enclosed within chromite, larger interstitial PGM and elongate aligned PGM – have Os isotope compositions that give Re-depletion model ages approximately equal to the age of the ophiolite at ~492 Ma. A number of other PGM – not confined to a single textural group – fall to more or less radiogenic values, with four PGM giving anomalously unradiogenic Os corresponding to an older age of ~1050 Ma. The $^{187}Os/^{188}Os$ isotopic ratios for PGM from Cliff and Quoys, from the same ophiolite section, are somewhat more radiogenic than those at Harold's Grave. This may be due to a distinct mantle source history or possibly the assimilation of radiogenic crustal Os.

# 1. INTRODUCTION

## 1.1 Platinum-group elements and Os isotopes in ophiolites

The study of the Re-Os isotopic system has become an important and widely used tool in investigations of mantle reservoirs and their evolution through Earth history. Owing to the mobility of Re during fluid interactions (e.g. Xiong, 2006), there is great benefit in measuring Os isotopes in situ in Re-poor grains to minimise uncertainties in correction for radiogenic Os ingrowth. Hence a number of studies (e.g. Walker et al., 2002b, González-Jiménez *et al.*, 2014) have taken this approach using Os-Ir rich phases in mantle rocks, particularly chromite-rich rocks in ophiolite complexes. Such IPGE enriched chromitites have attracted much interest since the advent of Os isotope analysis, in that they provide data points constraining the Re-Os mantle growth curve and provide insights into the evolution of mantle reservoirs with time (e.g. Shirey and Walker, 1998). However, the mechanisms by which IPGE are concentrated within ophiolitic chromite remain a matter of debate, resolution of which is critical for the interpretation of the isotope data.

Podiform chromitite in ophiolite complexes commonly hosts Ir-, Ru- and Os-bearing platinum-group minerals (IPGM) as for example in the Tiebaghi ophioite in New Caledonia (Page et al., 1982), various ophiolite complexes in Newfoundland (Page and Talkington, 1984), the Semail ophiolite (Augé 1986, Prichard et al., 1996; Ahmed and Arai, 2003), the Troodos ophiolite in Cyprus (Constantinides et al., 1980; Prichard and Lord, 1990), the Luobusa Ophiolite in Southern Tibet (Zhou et al., 1996), the Kamuikotan zone in northern Japan (Arai et al., 1999) and in the Vourinos and Orthrys ophiolites in Greece (Economou-Eliopoulos, 1996). *In situ* Os isotope measurements have been applied to a number of these. On the whole, as expected, minerals in ophiolites give Re-Os model ages that are the same as that of the formation of the oceanic crust that becomes the ophiolite on emplacement. Some model ages are much older and appear to record a history prior to ocean crust formation with inherited depletion ages from previous melting events. González-Jiménez et al. (2014) review the evidence from *in situ* analysis of individual platinum-group minerals in ophiolitic chromitites and demonstrate that such grains may have highly variable Os isotope compositions. In some cases they

show that variable isotopic composition occurs in PGMs located within the same thin section. Thus, in some ophiolitic chromitites the PGM found in a single chromite deposit may show a spectrum of compositions that could be interpreted as Re-depletion ($T_{RD}$) model ages. This poses an intriguing problem in the interpretation of such data.

Some of the highest concentrations of Ir, Ru and Us (IPGEs) are found in the Unst Ophiolite in Shetland. The Shetland ophiolite belongs to the relatively rare group of ophiolites having chromitites that contain elevated Pt, Pd and Rh (PPGE). Examples of these PPGE enriched ophiolitic chromitites include Thetford Mines in Canada (Corrivaux and Laflamme, 1990), Leka in Norway (Pedersen et al., 1993), Albanian ophiolites (Ohnenstetter et al., 1999), Al 'Ays in Saudi Arabia (Prichard et al., 2008a), Bragança in Portugal (Bridges et al., 1993), Pindos in Greece (Prichard et al., 2008b), Pirogues in New Caledonia (Augé et al., 1998), Acoje in the Philippines (Bacuta et al., 1988; Orberger et al., 1988) and Berit in Turkey (Kozul et al. 2014). Chromitites from the Shetland ophiolite belong to the IPGE and PPGE enriched group, with all six PGE being present at µg/g levels. Prichard et al. (2008a) and Prichard and Brough (2009) concluded that the Shetland chromitites formed from magmas that were close to sulfide liquid saturation, resulting in local accumulation of traces of strongly PGE-enriched sulfide liquid.

The Shetland occurrences, particularly the very highly IPGE enriched chromitites at Harold's Grave (Fig. 1), provide an opportunity to investigate the processes that lead to IPGE concentration and IPGM crystallisation in ophiolitic chromitite and also to investigate the detailed controls on the variability of Os isotope signatures at grain scale. In this contribution, we use detailed 2D and 3D petrographic observations at high spatial resolutions to address the grain-scale spatial distribution of PGM within the Harold's Grave chromitite. This is the first time that grain-scale 3D spatial information has been combined with *in situ* Os isotope data to investigate the origin of the IPGE enrichment and PGM formation and also the extent of grain scale isotopic heterogeneity and its significance. Our conclusions have implications for the phenomenon of PGE concentrations in ophiolitic chromitites and the mechanisms of concentration of PGEs in Reef-type deposits in layered intrusions, and also provide significant insight into the broader behaviour of the PGEs in mantle processes.

### 1.2 Platinum-group elements in the Shetland ophiolite

The Shetland ophiolite is exposed in obduction nappes on Unst and Fetlar, the most northerly islands of the Shetland Islands, NE of the Scottish mainland, UK. The lower parts of an ophiolite sequence are preserved with mantle harzburgite overlain by crustal dunite, wehrlite and clinopyroxenite. In turn these lithologies are overlain by gabbro, with dyke swarms above that mark the base of the sheeted dyke complex (Flinn, 1985; Prichard, 1985). The formation of the ophiolite occurred in an

ocean that opened at about 600 Ma and closed at about 500 Ma, obducting the ophiolite which was then affected by the intrusion of the Skaw granite in northern Unst at about 425.6 Ma (Flinn and Oglethorpe 2005). A zircon U-Pb crystallisation age of 492±3 Ma from an anatectic plagiogranite vein is accepted as the likely crystallisation age of the ophiolite, which was emplaced during closure of the Iapetus Ocean in the Grampian orogeny at ~470 Ma (O'Driscoll *et al.*, 2012).

The ophiolite hosts podiform chromitites surrounded by a dunite envelope in mantle harzburgite. Two of these, within the Baltasound area on Unst (Fig. 1), have particularly anomalously high ug/g values of PGEs: The Cliff locality is extremely enriched in Pt, Pd and Rh compared with ophiolitic chromitites worldwide; whereas, in contrast, the Harold's Grave locality is IPGE enriched (Table 1), both containing total PGE concentrations in excess of 60 ug/g (Prichard and Lord, 1993). The PGE concentrations in the ophiolite and the history of their discovery are summarised in Brough et al. (2015). Detailed petrogenetic studies of the various chromitite pods within the Baltasound area highlight significant short-range variability in chemical and Os isotopic characteristics, implying derivation for a source with short-range heterogeneity feeding magmas through a series of distinct conduits (O'Driscoll et al., 2012; Derbyshire et al., 2013).

**1.3 Platinum-group elements and chromitite at Harold's Grave**

The Harold's Grave chromitite is located to the north of Baltasound, west of the road from Baltasound to Haroldswick (Fig. 1), within one of the largest dunite lenses in the mantle section of the ophiolite. The chromitite has been quarried and now is present mostly in spoil tips beside a quarry that is 15 m long and 2-3 m wide. However the surrounding dunite contains a few thin layers of chromitite that are still preserved *in situ*. The boulders of spoil show that the chromitite forms parallel layers a few cm thick and around 10 cm apart, separated by dunite. These chromitite layers are typically folded and fractured.

The composition of the chromitite at Harold's Grave has been shown to be distinct from the other chromitites in the ophiolite, having lower Mg#, a lower $Fe^{3+}/Fe^{2+}$ ratio and elevated concentrations of $TiO_2$, $V_2O_5$ and Zn. These features are consistent with low oxygen fugacity conditions that favour the precipitation of the IPGE into PGM, due to the reduced solubility of the IPGE in silicate melts (Borisov and Palme, 1995, 2000; Brenan and Andrews, 2001; Brenan et al., 2005). Chromites imaged using high resolution X-ray computed tomography display distinctive stepped "hopper" grain boundaries suggestive of rapid crystallisation (Prichard et al., 2017). Analysis of eight chromitites from Harold's Grave suggests that the chromitite is consistently enriched in IPGE with values ranging from 2-7ppm Ru, 1-3ppm Ir and 0.6-3 ppm Os. PPGE are also concentrated in these chromitites but at lower levels than the IPGE with ranges of 420 - 785 ppb for Pt, 257-422ppb for Rh and even lower

values of 36-69 ppb for Pd. The samples chosen to study in this current research were those analysed for whole rock PGE as described in Brough et al. (2015) (Table 1).

Fig 1

**1.4 Platinum Group Minerals in the Shetland ophiolite**

There has been a number of studies of PGM in the Shetland ophiolite. PGM located in different stratigraphic levels and in different chromitite pods within the mantle have been summarised in Prichard et al. (1994). (Note that we follow the convention of using the abbreviation PGM to refer to platinum-group-element dominant minerals, PGE to refer to the elements, IPGE to refer to Ir, Ru and Os, and IPGM for IPGE dominated minerals). PGM in the Cliff and Harold's Grave chromitites are described in Prichard and Tarkian (1988) and Tarkian and Prichard (1987). At Cliff the PGM assemblage consists of sperrylite $PtAs_2$, stibiopalladinite $Pd_5Sb_2$, hongschiite PtCu, PGE and Au alloys, potarite PdHg, and Pt- and Pd-oxides as well as Os-, Ir- and Ru-rich PGM (IPGM) including laurite ($RuS_2$), irarsite (Ir,Ru, Rh,Os)AsS, hollingworthite (Rh,Pt,Pd)AsS, and native Os all accompanied by ruthenian pentlandite (pentlandite with > 50 mg/g Ru). Except for Harold's Grave, the rest of the chromitite pods in the mantle harzburgite are not enriched in PGE above the 10-100 ng/g levels expected for most podiform chromitites. Occasional composite grains of PGM do occur, as in the chromitite pod at Nikkavord North which contains clusters of laurite, irarsite, hollingworthite, ruthenian pentlandite, Ni-Rh antimonide and native Os (Prichard et al. 1986). In sulfide-bearing dunites associated with chromitites, which form the crustal sequence overlying the mantle harzburgite, PGM include Pt-, Pd-rich stibiopalladinite $Pd_5Sb_2$, geversite $Pt(Sb,Bi)_2$, genkinite $(Pt,Pd)_4Sb_3$, Pt-Fe-Cu alloys and Pt- and Pd-oxides. The wehrlite contains a mineral assemblage formed from a more fractionated magma consisting of Pd-Cu sulfide and Pd-Pb alloys $\pm$ Pt and $\pm$ Au in unaltered clinopyroxenite, with Pt and Pd arsenides, antimonides and tellurides in adjacent serpentinite.

Arsenic- and Sb-bearing PGM are only found interstitial to the chromite grains and thus are associated with the serpentine rather than with melts associated with crystallisation of the chromite (Prichard et al. 1994). It has been suggested that the addition of the As and Sb occurred late as the ophiolite was emplaced and demonstrated by the presence of As up to 1% in serpentinites along the basal thrust contact (Prichard and Lord, 1993). Thus for example the sperrylite at Cliff is a late PGM formed by alteration of a primary PGM assemblage.

**1.5 Platinum Group Minerals at Harold's Grave**

Studies of the IPGE mineralogy at Harold's Grave have revealed an assemblage dominated by laurite, ruthenian pentlandite (defined as pentlandite with >30 mg/g Ru), native Os and irarsite often

rimmed by hollingworthite. Other minerals recorded include genkinite, hongschiite, stibiopalladinite and an unnamed Rh-Ni-Sb (Prichard and Tarkian, 1988).

There textural associations of the PGM are similar to those observed in other Shetland chromitites. Euhedral Os-bearing laurite grains are included within the chromite grains, whereas Os-barren laurite of irregular shape is found where the laurite is in contact with the serpentine interstitial to the chromite grains. This interstitial laurite is often accompanied by native Os, irarsite and ruthenian pentlandite forming composite PGM; the PPGE-bearing PGM are predominantly interstitial to the chromite grains (Prichard et al. 1986; Tarkian and Prichard, 1987; Prichard et al. 1994). This PGM assemblage described from the Harold's Grave chromitite was the subject of an Os-isotope study by Badanina et al. (2016) with the observation that there are composite grains of laurite and Ru-Os-Ir alloys within the chromite grains. These authors also observed that the PGM within the chromite grains are smaller than those in interstitial positions.

### 1.6 Osmium isotopes in the Shetland ophiolite

There have been three previous studies of Os isotopes in the Shetland ophiolite. The first analysed whole rock powders of chromitites resulted in $^{187}Os/^{188}Os$ values of 0.12523 for Harold's Grave, 0.12721 for Cliff, 0.12645 for a chromitite in the crustal dunite and 0.12790 for Quoys (Walker et al. 2002b). A further study on whole rock chromitites and peridotites from the ophiolite found Re-Os isotope model ages of approximately 500 Ma as well as an earlier Mesoproterozoic melting event (O'Driscoll et al. 2012). A third study examined Os-bearing minerals in situ in a chromitite sample from Harold's Grave (Badanina et al. 2016). That study found that PGM interstitial to chromite grains generally displayed a range of $^{187}Os/^{188}Os$, from 0.1235 to 0.1250, that is indistinguishable from those included in chromite. They interpreted this as preservation of the ratios during alteration and serpentinisation in a closed isotopic system; with PGM enclosed in chromite grains representing a magmatic assemblage and interstitial PGM representing an alteration assemblage.

The study presented here combines in situ Os isotope measurements with the 3 dimensional location of PGM, following the methodology of Godel et al. (2010, 2014), to investigate the genesis and histories of each group of PGM at Harold's Grave. This approach has been further extended to Os-bearing PGM from the Cliff, Quoys and Nikkavord South chromitite lenses in the mantle of the Shetland ophiolite complex.

## 2. MATERIAL AND METHODS

Six micro-cores were drilled from samples of Harold's Grave chromitite and were scanned using the XRADIA XRM 500 high-resolution 3D X-ray microscope system at the Australian Resources Research Centre (CSIRO Mineral Resources, Kensington, Western Australia). The characteristics of the micro-

core, voxel sizes and number of projections used to volume reconstruction are provided in supplementary Table S1. The instrument was set-up (for each sample) to maximise phase contrast between chromite, Ru-pentlandite, the platinum-group minerals and sillicates. For long samples (HG6A and HGS), multiple tomographies were recorded along the vertical axis and stitched in 3D to provide an entire view of the samples. Chromite, silicates, Ru-pentlandite and PGM were segmented from the greyscale volumes using modified gradient watershed algorithm described in Godel (2013). Quantitative measurments (spatial location, volume, equivalent sphere diameter referred to as ESD, maximum and minimum Feret lengths, sphericity and 3D orientations of the elongation axes) were calculated for each PGM. These informations were used relocate PGM during the grinding and polishing processes to expose the PGM and perform their chemical and isotopic characterisation. It should be noted that PGM of size smaller than the spatial resolution (Table 2) were not quantified using the HRXCT.

The PGM were identified using a Cambridge Instruments (ZEISS NTS) S360 scanning electron microscope (SEM), coupled to an Oxford Instruments INCA energy plus which included both an energy dispersive (ED) and a wave dispersive (WD) X-ray analytical system at Cardiff University. Chromite grains were analysed with a 20kV accelerating voltage, 20 nA beam current and fixed beam size (approximately 10-15 nm) with a live-time of 50 s for ED. A cobalt standard and separate chromite standard were used to monitor for instrumental drift. Many PGM (about 2,000) were analysed qualitatively but a few typical common ones and the rarer ones were analysed quantitatively.

Osmium-bearing PGM were analysed for $^{187}Os/^{188}Os$ by laser ablation MC-ICPMS, using a New Wave UP 213 nm Nd:YAG laser system, coupled to a ThermoFinnigan Neptune MC-ICPMS at Durham Geochemistry Centre, Durham University. Full details are given in the Appendix.

## 3. RESULTS

### 3.1 Five Generations of PGM

Overall five generations of PGM have been identified from the 3D volumes. These five groups consist of (i) small (1-22 μm ESD) laurites often with IPGM enclosed in chromite grains, (ii) larger composite PGM hosting all 6 PGE, sometimes forming clusters, located either in serpentinized zones cross cutting chromite grains or on the edge outside chromite grains (referred to hereafter as interstitial grains) with individual composite PGM reaching 350 μm ESD, and about 10% (in number) of grains exceeding 100 μm. (iii) aligned elongate PGM (up to 100 μm in length), occurring within a few chromite grains (hosting all PGE except Pd) (iv) almost spherical laurite (80 μm ESD) grains in a sheet

cross cutting a chromitite layer, and lastly (v) small (10 μm ESD) elongate PGM associated with micro-shearing. The numbers and size range of PGM imaged in the different scans is shown in Table 3.

### *3.1.1 Group (i) IPGM hosted within chromite*

Group (i) PGM are those enclosed by the chromite grains and are the smallest PGM imaged. In 3D the PGM can be seen to form single equant grains or composite grains of equant and elongate PGM (Fig. 2 A-F, supplementary Fig. S1). The PGM are hosted within the chromite, not associated with the silicate inclusions that are also present within the chromite grains, and not associated with fractures. They are evenly distributed as shown by Fig. 2 G and H.

Fig 2.

A study of HG6 showed that within the chromite grains the PGM are almost exclusively equant laurite and elongate Os-Ir-Ru-Rh alloys with only two Pt-bearing PGM that form part of composite PGM. These PGM are small with laurite ranging from 0.5 x 0.5 μm to 10 x 8 μm in diameter and averaging 4.8 x 3.9 μm in diameter, whereas the Os-Ir-Ru-Rh alloys range from 0.5 x 0.5 to 6 x 3 μm in apparent cross section diameter with an average of 3.4 x 2.2 μm. The number and area of PGM exposed on a 2D slice surface of HG6 are documented according to textural position and composition in Table 3 and Figs. 3 and 4. Energy-dispersive SEM analyses of the PGM are given in Supplementary Table S2.

Fig 3

Fig 4

### *3.1.2 Group (ii) PGM interstitial to chromite grains*

The PGM in this group are interstitial to chromite, usually located on the edges of the grains, and occur in HG1, HG6, HG7, HG8 and HGS. Imaging in 3D appears to suggest that some large composite PGM are located within a single chromite grain, but EBSD analysis of the area around one PGM indicates that the surrounding chromite is in fact composed of 5 grains, and the PGM is located at the junction of two grains (Fig. 5, supplementary Figs. S2, S3). This suggests that other such PGM may also be located at the junctions of adjacent chromite grains, rather than being enclosed.

Fig 5.

These PGM have a very different composition to those in Group (i) (Supplementary Table S3) and are much larger and more abundant. A survey of HG6 revealed the variety of PGM in this group (Fig. 3). In contrast to the small laurite crystals and associated IPGM alloys enclosed in chromite belonging to Group (i), interstitial PGE-bearing minerals are more varied with predominantly laurite associated with native Os, irarsite and ruthenian pentlandite. Os-Ir alloys are a minor component of this

assemblage and the IPGM are accompanied by Pt-bearing PGM; small 1-2 μm PGMs are predominant in terms of numbers of grains, but minor in terms of total volume or area (Fig. 3).

The interstitial IPGM and ruthenian pentlandite (Fig. 7) are accompanied by Rh-Pt-Ni- antimonides, hollingworthite that rims irarsite, platarsite, Pt-Fe alloy and sperrylite. Os-poor laurite is commonly rimmed by Os-rich laurite. Rare oxidised PGM have been located: one Ru-oxide and one precursor Rh-Pt-Ni- antimonide. Millerite and heazlewoodite are relatively common, forming composite grains with IPGM. One grain of digenite was located (Fig. 7 I) as well as one grain of chalcocite and an unnamed silver copper sulfide, but Cu-bearing minerals are extremely rare. The abundance and area of different PGM, both enclosed in chromite and interstitial, is shown for each sample in Supplementary Figure S1.

The imaged part of HG6 hosts one unusually large composite PGM grain, having a maximum diameter in 3D of 200 μm (Fig. 9) and shown to be 110 x 100 μm in diameter as exposed in the slice in 2D. This PGM consists of laurite, ruthenian pentlandite, irarsite and native osmium.

Fig 6.

The largest group or cluster of PGM that was imaged occurs in HG7 (supplementary Fig. S3) and extends over a volume of about 1 $mm^3$. The PGM in this group are entirely interstitial to the chromite grains. In addition to the 3D image, this was verified by the examination of textural location of PGE-bearing minerals in 25 2D polished slices through the cluster (3D image and chart of PGM abundances in supplementary Figs S2, S3). The PGM and ruthenian pentlandite are wrapped around two chromite grains to form an 'S' shaped cluster (3D image and chart of PGM abundances in supplementary Figs S2, S3). Fifteen hundred PGM were located and analysed in this cluster. They include many composite PGM and all 6 PGE including most abundantly ruthenian pentlandite and irarsite but also the PGE-arsenides sperrylite, hollingworthite and platarsite, as well as laurite, Pt alloys and oxides, native osmium, rarer PGE antimonides and rare Pd-PGM, reflecting the low values of Pd in the whole-rock PGE analyses.

### *3.1.3 Group (iii) PGM aligned within chromite grains*

Detailed observation of the 3D morphologies of PGM reveals local clusters of large (50 μm) elongate rod shaped grains with a distinct preferred orientation, enclosed within particular host chromite grains (Fig. 7). EBSD analysis of a chromite containing five PGM grains with mutually parallel long axes shows that the host chromite is a single crystal. PGM from this grain were analysed on sections cut through these PGM, and they were found to consist of composite PGM of native Pt and native Os, IrSbS (possibly tolovkite), laurite, irarsite and a Pt-Rh-Ni-antimonide representing all the PGE except Pd (supplementary Fig S1).

Fig 7 3d aligned PGMs

*3.1.4 Group (iv) PGM in a sheet crosscutting a chromitite layer*

A 3D tomography image of HGS, a chromitite taken from a small 2 cm thick in situ layer, showed the presence of 237 PGM within approximately 100 $mm^3$ volume of rock, including several large (80 µm) almost spherical PGM in a sheet traversing the layer at an angle of approximately 60 degrees to its margins (Supplementary Fig. S4). SEM EDS analysis of these PGM within the sheet showed that they are laurite with small inclusions of Os-Ir alloys, irarsite, Rh antimonide and one Ni-Fe-sulfide.

*3.1.4 Group (v) deformed PGM*

The Harold's Grave chromitites are folded (Brough et al. 2015) and cut by narrow shear zones. These samples show some evidence of this. For example HG6A displays at least 2 stages of local narrow zones of shearing. Even the PGM in these shear zones are deformed (supplementary fig s4). Such shearing of PGM is observed in 2D polished thin section but in 3D the deformation is more clearly observed in one case where the PGM (having probably once been a large composite PGM) are strung out in a line along the shear plane. The individual PGM in this shear are also elongated in a direction that is parallel to the shear-related lineation in the surrounding chromite (Fig. 15 C).

## 3.2 Os isotopes

Overall, initial $^{187}Os/^{188}Os$ data (n=90) for 2D- and 3D-imaged PGM in the Harold's Grave chromitite display a range of $^{187}Os/^{188}Os$ from 0.118 to 0.133 , with all but five being sub-chondritic. They define a clear modal peak at around 0.1250, with 67 of the 90 PGM falling within uncertainty of the modal range, 0.1245-0.1255 (Fig. 8; see supplementary materials Table S4 for results; correction for ingrowth of $^{187}Os$ is never larger than 0.00009 due to very low Re/Os). This modal peak matches whole-rock chromitite compositions from Harold's Grave (O'Driscoll et al., 2012; Walker et al., 2002b) and corresponds to a range of Re-depletion ($T_{RD}$) ages from 325 to 600 Ma, with a peak at ~470 Ma, based on an ordinary (O) chondrite mantle Re-Os growth curve (present day $^{187}Os/^{188}Os$ = 0.1283, $^{187}Re/^{188}Os$ = 0.422; Walker et al., 2002a), which is close to the formation age of the ophiolite (U/Pb in zircon from a cross-cutting plagiogranite gives a minimum age of ~492 Ma; Spray and Dunning, 1991). Use of a primitive mantle growth curve (Meisel et al., 2001) results in a considerably older age of ~650 Ma. Most PGM belonging to groups (i) and (ii) have the same modal age close to 492 Ma. Four of the five Group (iii) PGM have this $^{187}Os/^{188}Os$ modal value, with the other having the most radiogenic ratio recorded of 0.133, giving a future age.

Fig. 8. Os isotope data compilation

The main modal range of $^{187}Os/^{188}Os$ is similar to a previously published PGM range mainly between of 0.124 and 0.125 (Badanina et al., 2016), although our modal peak is approximately 0.0005 higher

than that previous study. There is no clear analytical reason for this, so we suggest that it may be a sampling effect, given that their range in encompassed by ours. The large range of $^{187}Os/^{188}Os$ within the modal peak, and the tails to older and younger (occasionally negative) $T_{RD}$ ages, emphasises that Os model ages are most robust where large datasets are available, and individual ages in small datasets carry significant uncertainty as to their meaning.

Lower $^{187}Os/^{188}Os$ ratios also occur, with a cluster between 0.1200 and 0.1215 (n=4), and several others between 0.122 and 0.123 (n=6). Some PGM with these lower ratios occur in the same polished section of chromitite as those with higher ratios; for example, two PGM from HG3 with similar locations (largely surrounded, but not completely enclosed within chromite) and both consisting of laurite, native Os and irarsite (probably group ii), have differing $^{187}Os/^{188}Os$ of 0.1208 and 0.1247. Thus, apart from their lower Os isotope ratios, these PGM are indistinguishable from some PGM whose model ages correspond to the age of the ophiolite. Most PGM with lower $^{187}Os/^{188}Os$ ratios of 0.120-0.122 are enclosed in chromite (Fig. 17), while all are composite grains with laurite and in four cases are associated with Rh-bearing PGM (Fig. 17 A-L). One composite PGM gives an even lower $^{187}Os/^{188}Os$ ratio of 0.1183 (Fig. 17 M and N). This composite PGM (consisting of laurite, irarsite and native Os, partially surrounded by millerite) is unlike all the other PGM located at Harold's Grave because it is located entirely enclosed in serpentine, more than 100 μm from the nearest chromite grain. Almost all other interstitial PGM are either attached to the edge of a chromite grain or are within ~10 μm.

There is a slight difference in the distribution of Os isotope values between enclosed and interstitial PGM. A slightly lower proportion of 68% of enclosed PGM (both groups (i) and (iii), n = 41), fall within uncertainty of the overall modal range. This compares to 75% of interstitial PGM (n = 16) and 80% (n = 25) of PGM that could not be definitively categorised, but are likely in many cases to have been in contact with melt external to chromite.

Only a very limited Os isotope dataset for PGM from other Shetland chromitites is presented here. Four PGM – one from Cliff and three from Quoys – gave $^{187}Os/^{188}Os$ values of 0.1270 - 0.1272 (Fig. 18). Using an O-chondrite evolution model, these ratios equate to Re-depletion ages between 150 and 175 Ma, younger (more enriched/less depleted) than those from Harold's Grave. One additional PGM from Cliff, a laurite in serpentine, gave a future age ($^{187}Os/^{188}Os$ = 0.1300). The less radiogenic PGM from Cliff matches one bulk chromitite from that locality (Walker et al., 2002b), but a later study indicates that individual chromitites, even from the same locality, may have variable $^{187}Os/^{188}Os$ (0.1292; O'Driscoll et al., 2012).

## 4. DISCUSSION

365 **4.1 Locations and formation of the PGM**

366 Harold's Grave chromitites contain abundant PGM, and the assemblage is dominated by IPGE-
367 bearing minerals. 3D imagery allows us to determine whether the PGM are completely enclosed in
368 chromite grains or whether they have had direct contact with interstitial melt and minerals. This
369 observation is very difficult to confirm any other way. PGM observed in 2D on polished thin sections,
370 or obtained by a mineral separation technique, do not have enough textural information to allow
371 these conclusions to be reached. The PGM in Group (i) are totally enclosed by the chromite and
372 usually not associated with large silicate inclusions, with rare exceptions (Fig. 2C). Equally it is
373 possible to confirm that the PGM within the cluster identified in HG7 are completely external to the
374 chromite grains. This provides us with unambiguous spatial constraints on distinct origins of the
375 PGMs in terms of the five groups delineated above, of which Groups (i) and (ii) account for the vast
376 majority of grains imaged and analysed.

377 *4.1.1. Magmatic laurite and IPGE alloys of Group (i)*

378 The Group (i) PGM consist of small grains of laurite sometimes attached to Os-Ir-Ru alloys that form
379 composite PGM all totally enclosed by chromite. These PGM are ubiquitous within the chromite
380 grains. The PGM in Group (i) probably crystallised directly from the magma as the chromite grains
381 crystallised. Such PGM have been produced experimentally (Brenan and Andrews, 2001) and
382 proximity to the surface of the chromite is thought to induce IPGM formation due to a lowering of
383 oxygen fugacity in boundary layers around growing chromite crystals, thus reducing the solubility of
384 the IPGE in silicate melt (Finnigan et al. 2008). Brenan and Andrews (2001) observed that both
385 laurite and Ru-Os-Ir alloys may occur, with alloys reducing in proportion as temperature falls and as
386 sulfur fugacity increases.

387 *4.1.2. Interstitial PGM clusters of Group (ii)*

388 The Group (ii) PGM association largely accounts for the distinctively high IPGE contents of the
389 Harold's Grave chromitite. It is also the most challenging to explain, particularly in view of the fact
390 that the modal Os isotope compositions of groups (i) and (ii) show a high degree of similarity. PGM
391 belonging to Group (ii) are all external to the chromite grains, usually in composite grains that
392 contain more than two PGM. Sometimes they form in polymineralic clusters, this being
393 demonstrated most clearly in HG7. The assemblage is IPGM dominated along with ruthenian
394 pentlandite but also variably present are Pt-Rh-dominant PPGM, rare Pd-PPGM, minor Ni-bearing
395 PGM and very rare (only 3 grains located) Cu sulfides. Based on their larger size and distinctly
396 different chemistry, group (ii) PGM clusters are clearly not simply altered equivalents of the enclosed

Group (i) PGM assemblage (as inferred by Badanina et al., 2016) and they imply a distinctly different petrogenesis.

Group (ii) PGM occur in clusters of multiple composite grains containing a small but consistent proportion of sulfide minerals. This suggests an initial magmatic PGE concentration mechanism akin to that proposed for the unusually PGE-enriched chromitites at Cliff: initial collection of PGE from a PGE-enriched magmatic sulfide component. This at Cliff was followed by a postulated episode of hydrothermal upgrading and S loss (Prichard et al., 1994). However, a simple hypothesis of sulfide collection of the PGE at Harold's Grave fails on a number of grounds: very high Pt/Pd ratios due to low Pd; a very low Cu content; and a sulfide assemblage dominated by Ru-rich pentlandite and a complete absence of pyrrhotite or pyrite. (Unmodified Ni-bearing magmatic sulfide assemblages always contain a component of Fe-sulfide as well as pentlandite, as a consequence of the restricted range of metal/S ratios in magmatic sulfide liquids – Naldrett 2004). The high metal/S ratio of the assemblage as a whole, as well as the absence of Cu, could potentially be explained by driving off S as a mobile component in late magmatic fluids, during interaction between chromite and sulfide (Naldrett et al., 1989) or during post-magmatic alteration. However, such a process fails to explain the very high Pt/Pd ratio, since simple S loss would be expected to leave the residual sulfide component strongly enriched in both Pt and Pd, as in the UG2 chromitites considered by Naldrett et al. (2009). Hydrothermal alteration related to serpentinisation of the host ultramafic rocks is very unlikely to preferentially remove Pd over Pt, on the evidence from komatiites that Pt and Pd are essentially immobile in serpentinising fluids (Barnes and Liu 2012). Unlike Cliff and crustal dunite chromitites, where native Cu indicates the altered remains of Cu sulfides (e.g. Prichard et al. 1994), there is an absence of native Cu at Harold's Grave. Finally, any process of S loss would also have to efficiently remove Re, to account for the almost complete absence of Re in the Group (ii) clusters analysed (all but two PGM have Re/Os <0.0065, and all are <0.06).

As an alternative, we consider the possibility that the Group (ii) association may have formed by direct precipitation of an assemblage of solid Os-Ir, Ru, Rh and Pt phases as a result of saturation of the parent silicate melt in these phases, in the absence of sulfide. However, this model has a number of major flaws. Firstly, it would require that these phases nucleated after cessation of chromite growth, rather than forming a crystallisation continuum with the enclosed population of Group (i) PGMs. It would require that these phases grew by a very efficient process of heterogeneous self-nucleation to create the clusters, in contrast to the nucleation of the isolated laurite grains now preserved within the chromite. There is no obvious reason why this change in nucleation style would take place, and why it would be so particularly effective at this one locality. Furthermore, this model then requires an additional ad hoc explanation for the sulfide component.

We therefore return to a sulfide collection model, but an additional process is required to account for the observed discrepancies. This process may be PGM formation during re-dissolution of an original PGE-rich cumulus magmatic sulfide component. We base this model on a combination of three independently published ideas for behaviour of PGEs in magmatic sulfides: upgrading of PGE within sulfide liquid by partial re-dissolution into sulfide-undersaturated magma (Kerr and Leitch, 2005); saturation of sulfide liquid with respect to IPGE alloys during partial melting of sulfide-bearing mantle (Fonseca et al., 2012); and stabilisation of PGE alloy during desulfidation of magmatic sulfide assemblages under conditions of declining sulfur fugacity (Peregoedova et al., 2004). The model of Fonseca et al. (2012) is especially applicable to the problem at hand.

During the process proposed by Fonseca et al. (2012), the initially solid mantle sulfide assemblage first melts, then progressively dissolves into the increasing volume of silicate partial melt with progressive melting of the mantle silicates. As a result of the extreme partition coefficients for PGEs into magmatic sulfide liquid (Mungall and Brenan 2014) the remaining sulfide liquid retains the entire PGE budget of the original source composition, and consequently becomes progressively enriched in PGE as the mass of sulfide drops. Close to the point at which the sulfide dissolves out entirely, the PGE content of the sulfide liquid increases rapidly to the point where it becomes saturated in PGM phases: Os-Ir alloys (Fonseca et al. 2012) and potentially also Pt-Fe alloy (Mungall and Brenan, 2014). With higher degrees of partial melting, the remaining sulfide completely dissolves into the silicate melt, which is now also constrained to be saturated in the same solid PGM phases. The solid PGM phases that precipitated from the sulfide component remain behind in the restite.

A closely analogous process may have operated within the Harold's Grave chromitites, which are of course sulfide-bearing mantle rocks themselves. The PGE distribution, i.e. the presence of Pt-Pd enriched as well as IPGE enriched chromitites, within the Shetland ophiolite as a whole implies that the ophiolite belongs to the type formed from magmas on the cusp of sulfide saturation (Prichard et al., 2008a), such that the same deposition site may have been fed over time by both sulfide-saturated and sulfide-undersaturated magmas. A MORB type magma was proposed to have formed the chromitite at Harold's Grave (Brough et al. 2015) and re-dissolution may have been caused by a new S-undersaturated pulse of silicate magma probably of a more boninitic composition. This view is supported by the presence of boninitic and MORB-like dykes intruded into the upper parts of the gabbro in the Shetland ophiolite (Prichard and Lord, 1988).

We propose that re-dissolution of sulfide took place at Harold's Grave, giving the following hypothetical sequence of events (Fig. 9).

Fig. 9.

1. Crystallisation of chromite from a magma saturated in both chromite and laurite, giving rise to formation of the Group (i) assemblage; laurite grains nucleate in redox boundaries layers around the growing chromite grains, as demonstrated in experimental studies by Finnigan et al. (2008).
2. Deposition of sulfide liquid droplets from transiently sulfide-saturated chromitite-forming liquid. These sulfides form at very high silicate/sulfide liquid mass ratios (R) giving rise to very high PGE, Ni and Cu contents in the sulfide liquid. Such Ni-Cu-rich sulfide melt compositions are potentially non-wetting against chromite, accounting for the dominant presence of the droplets interstitial to chromite rather than enclosed within them (Brenan and Rose, 2002). High R factors are the necessary consequence of co-precipitation of sulfide with chromitite: owing to the low solubility of chromite in mafic magmas, the chromite itself requires hundreds to thousands of times its own volume of magma to grow. The inferred original sulfide abundance in the rock (and in sulfide bearing chromitites in general) is much less than 1%, i.e. hundreds of times less than the chromite abundance; hence sulfides achieve R values potentially as high as millions, giving rise to PGE tenors as high as percent levels, calculated from the Campbell and Naldrett (1979) R-factor equation assuming initial abundances of the order of 10 ppb in the silicate magma.
3. Continuing influx of sulfide-undersaturated, superheated magma through the accumulation site of the chromitite causes re-dissolution of the sulfide component, further upgrading the PGE content of the sulfide liquid (Kerr and Leitch 2005) and giving rise to an analogous sequence of events as that proposed by Fonseca et al. (2012) for partial melting of sulfidic mantle rocks. In this case, though, the sulfides are extremely PGE-enriched to begin with and at or very close to saturation in solid IPGM and Pt-Fe alloy. As the PGE tenors are driven upward within the diminishing volume of sulfide liquid, PGM saturation is attained and PGM phases nucleate and grow within the sulfide liquid, forming clusters or composite grains (Fig. 9 G). The sulfide liquid component, carrying Cu, Ni, Pd and Re, eventually dissolves completely back into the silicate melt, leaving behind nothing but solid PGM. Of the PGE, only Pd is preferentially lost to the silicate melt owing to its inability to form solid PGM at magmatic temperatures (Mungall, 2014). The relative depletion of Pt over the IPGE is explained by a higher Pt solubility in silicate melt (Mungall and Brenan 2014), such that Pt alloy forms very close to the sulfide disappearance point (Fig. 20G). The result is the formation of the Group (ii) PGM associations, with the distinctive weakly Pt-depleted and strongly Pd-depleted PGE patterns. These (clusters) subsequently undergo post-magmatic alteration to form the presently preserved mineral assemblage, retaining non-radiogenic Os

isotopic compositions owing to efficient removal of the Re-bearing component at the magmatic stage.

This mechanism explains many features of the Group (ii) interstitial mineral association, but still leaves a problem that requires further explanation: the common presence in the Group (ii) assemblages of ruthenian pentlandite. If this phase is derived from incompletely re-dissolved sulfide melt, then this melt component should also have retained Pd and Re. As we have noted, the Group (ii) PGM associations contain almost no Re. Four possible explanations have been considered.

1. The sulfide dissolution process takes place at a temperature within the melting range of the sulfide, such that solid Ni-rich monosulfide solid solution (MSS) is stable and retained in the source, while the residual Cu-rich melt is re-dissolved or physically entrained and removed, as proposed by Ballhaus et al. (2006) to explain PGE fractionation during mantle melting. This explanation is not favoured, as it would still involve retention of Re in the MSS component, owing to the partition coefficient for Re into MSS from sulfide liquid being greater than unity (Brenan, 2002). It is possible that the melt may have been Re poor owing to melting during oxidizing conditions (Fonseca, pers comm. 2016) but there is no evidence in the compositions of the chromite grains that the parent melts were unusually oxidised; high V contents in Harold's Grave chromite (Brough etal., 2015) implies the opposite.
2. A ruthenium- and Ni-rich sulfide PGM is stabilised within the contracting sulfide droplet at a higher temperature than the normal sulfide liquidus, possibly as a consequence of reaction of early formed laurite with highly Ni-enriched sulfide liquid. This phase is converted to Ru-pentlandite during low temperature re-equilibration and/or alteration.
3. The PGM aggregates formed by the process of complete re-dissolution of sulfide, then acquired their sulfide component by subsequent reaction between IPGM and infiltrating sulfide-saturated interstitial silicate melt. This process has been invoked by Barnes et al. (2016) to account for an association between primary magmatic Pt-rich PGM and small proportions of Ni-Cu sulfides.
4. The Ru-pentlandite is entirely a product of low-T alteration of laurite formed as part of the solid PGM assemblage. This origin of Ru-pentlandite, a widespread mineral in altered ophiolitic chromitites, has been proposed for example by Genkin et al. (1974). There is no textural evidence for this process here, however.

None of the mechanisms proposed are entirely satisfactory and are all (particularly explanation 3) somewhat ad hoc. Ru-pentlandite as a product of low-T alteration of laurite (explanation 4) is preferred for simplicity, and is consistent with previous interpretations of altered PGM assemblages,

but lacks textural evidence, while number 2 is more coherent with the overall model but would require experimental verification of the stability of a Ru-Ni-S phase at magmatic temperatures. Nonetheless, the sulfide re-dissolution model explains the bulk of the critical observations, and provides an intriguing link between Harold's Grave and other more general processes operating within the mantle and within chromitites in general.

We note that the very small difference in the distribution of Os model ages between the Group (i) enclosed and Group (ii) interstitial grains is consistent with a distinct derivation for the S-saturated and undersaturated magma components. The slightly less radiogenic interstitial component, derived from the S-undersaturated magma according to the model presented here, could have been derived from a mantle source with slightly lower time-integrated sulfide content, and hence a higher Os/Re ratio.

*4.1.3. Formation of the Group (iii) elongated aligned PGM*

Group (iii) PGM are distinct from the other groups in that they are entirely enclosed within chromite grains and aligned approximately parallel to each other within an individual chromite grain. They are considerably larger than Group (i) IPGM and they are composed of IPGM accompanied by Pt and Rh. These Group (iii) PGM may have formed in two ways:

1. Those elongate aligned PGM that occur only in a few grains of chromite may have crystallised along crystallographic planes of the chromite as it crystallised. One explanation comes from the experimental studies by Finnigan et al. (2008) as outlined above (section 4.2), which demonstrated that IPGM phases nucleate preferentially in anomalously reduced compositional boundary layers around growing chromite crystals. A redox gradient is generated in the boundary layer owing to the preferential partitioning of ferric iron into the chromite lattice; the resulting reduction of the silicate melt lowers the IPGE solubility, which is a very strong positive function of $fO_2$ (e.g. Borisov and Palme, 1995; Brenan and Andrews, 2001), which itself is defined by the $Fe^{3+}/Fe^{2+}$ ratio of the silicate melt. Finnigan et al. (2008) further suggested that such boundary layers might be best developed around chromite grains that were initially most chemically out of equilibrium with the host melt, such that particular grains might contain multiple IPGMs while other neighbouring grains contained none. This is consistent with the observations reported here for the Group (iii) PGM.
2. Alternatively, there is increasing evidence that PGE can be incorporated in solid solution within chromite as it crystallises and then be ejected on cooling. This has been invoked to explain IPGE-enriched chromite phenocrysts in volcanic rocks and in Bushveld marginal sills (Park et al., 2012; Pagé et al. 2012; Pagé and Barnes 2013 and 2016). Experimental studies

suggest that the IPGE and Rh have chromite-melt partition coefficients in the range 40 to 200 at fO2 around the Ni–NiO buffer (Brenan et al., 2012), and at higher fO2 (probably unrealistic for the case at hand) the values can approach 1000 (Righter et al., 2004). A recent study by Barnes et al. (2016) suggests that the IPGE entered in solid solution into the Stillwater chromite and then diffused into base metal sulfide inclusions forming laurite. The very enriched PGE whole rock compositions of chromitites at Harold's Grave require that PGE from a large volume of magma all collected in the small volume of chromitite in this particular dunite lens, the largest in the mantle harzburgite section of the Shetland ophiolite (Brough et al., 2015). It is possible therefore that chromites from Harold's Grave incorporated PGE into their structure and then on cooling these exsolved to form the parallel Group (iii) PGM observed in 3D. This interpretation would require that partition coefficients of Ru into chromite be considerably higher than the values indicated by Brenan et al. (2012), tending to favour explanation 1.

### 4.2 Alteration

The PGM assemblage that we observe today in these highly anomalous PGE-enriched samples from Harold's Grave is a secondary alteration assemblage; the primary assemblages having been overprinted during serpentinisation of the ophiolite especially during emplacement. The basement contact of the ophiolite is enriched up to 1% As (Prichard et al. 1993) swamping any magmatic As signature in these rocks. The late introduction of As and Sb on ophiolite emplacement has produced arsenides including sperrylite and those belonging to the irarsite, hollingworthite and platarsite solid solution series, and rarer antimonides including Rh-Sb and (NiRhPt)Sb (Supplementary material Table S3). Accompanying this alteration is the formation of abundant small 1-2 □m native Os grains within the composite IPGM interstitial to the chromite grains. Much of this Os is likely to have been derived from the alteration of Os-Ir-bearing laurite to pure $RuS_2$. Subsequent weathering has produced rare PGE-oxides such as the Ru-oxide observed in HG6 (Supplementary material Table S3). PGE-oxides have previously been observed in the Shetland ophiolite chromitites (Prichard et al. 1994). The Group (iii) PGM assemblage is also likely to be an alteration assemblage with the presence of PGM arsenides associated with late stage fluid influx along the sole thrust of the ophiolite (Brough et al., 2015). The Pt-Rh-Ni antimonide is also a characteristic mineral formed late with the introduction of antimony on ophiolite emplacement. The PGM alteration assemblages are very unlikely to have been remobilized into these aligned clusters of Group (iii) and are likely pseudomorphs of former PGM.

### 4.3. Osmium isotope constraints on chromitite and PGM formation

The existence of a large range of $^{187}Os/^{188}Os$ in Harold's Grave PGM, sometimes within single sections (as described in results), has previously been observed in the Mayarí-Cristal ophiolite, Cuba (Marchesi et al., 2011), where comparable differences in $^{187}Os/^{188}Os$ of 0.1185 to 0.1274 were found in a single sample and 0.1185 to 0.1232 between two PGM only millimetres apart. As the Re/Os ratios of the Harold's Grave PGM are uniformly low, variable in situ ingrowth of $^{187}Os$ cannot account for the isotopic variations. Such variable compositions, therefore, could either represent (a) inherited xenocrystic PGM; (b) pre-existing composition of the mantle through which the chromitite-forming melts percolated; (c) contamination of some, but few, discrete melts by both crustal Os (radiogenic) or lithospheric Os (unradiogenic); or (d) distinct mantle sources of percolating melts (e.g. Marchesi et al., 2011). No experimental constraints exist for PGM transport in percolating melts, but given the compositional and mineralogical similarity of PGM grains, regardless of their Os isotope signature, a xenocrystic origin of isotopic heterogeneity seems highly unlikely and would require extraordinary coincidence. Inheritance of the isotopic signatures from the in situ mantle also seems unlikely given the small size (3 x 15 m) of the chromitite outcrop and that individual potentially isotopically heterogeneous pre-existing sulfides (e.g. Harvey et al. 2006) would not contain sufficient Os to account for the Os budget of an individual PGM. Contamination cannot be ruled out, but is made less likely by the need for both radiogenic and unradiogenic contaminants that have only affected a small proportion of PGM-forming melts. Thus, the most plausible mechanism is the precipitation of isotopically heterogeneous PGM from discrete PGE-enriched melts percolating through chromitite, which in some cases have distinct mantle source histories.

This preservation of isotopically heterogeneous PGM requires their isolation from subsequent melt percolation. Gonzalez-Jimenez et al. (2012) found that interstitial PGM from the Dobromirtsi Ultramafic Massif, Bulgaria, show greater isotopic variation than those that are enclosed, which was interpreted to reflect the influence of metamorphic fluid flow. Contrary to their findings, isotopic heterogeneity is rarer in the interstitial PGM in our Harold's Grave samples, perhaps due to limited fluid flow. Nonetheless, it is notable that isotopic variations are present in both enclosed and interstitial PGM. This implies that (i) subsequent melts do not physically come into contact with the existing PGM, for example through the process of inclusion in chromitite which undoubtedly occurs (e.g. Fig. 3), and/or (ii) that the PGM are chemically unaffected by contact with the melt, at least in terms of exchange of osmium isotopes. Given the high Os contents of the PGM, and their stability in high temperature melt systems, chemical isolation is not unexpected (e.g. see Marchesi et al., 2011).

### 4.4. Long-term evolution of the source(s) of Shetland chromitites

Of the 83 separate PGM analysed (90 analyses) from Harold's Grave, 62 have $^{187}Os/^{188}Os$ ratios that fall within uncertainty of 0.1245-0.1255. Using an ordinary (O) chondrite reference model (Walker et

al., 2002a), the mode for the dataset (0.1250) corresponds to a Re-depletion age of ~470 Ma, which is similar to the formation age of the ophiolite (~492 Ma; Spray and Dunning, 1991). The strong mode within this dataset indicates that the melts that formed Harold's Grave chromitites, and the PGM they contain, came predominantly from the same mantle source, or at least sources with similar histories. Again assuming an O-chondrite model, this mantle was not strongly depleted or enriched, having gamma Os of close to zero (a mode of ~0.1) at 492 Ma (gamma Os is the deviation from the O-chondrite model in percent). If, however, the more radiogenic primitive mantle evolution model is used (Meisel et al., 2001), then the modal composition would reflect a source with moderate long-term depletion (sub-chondritic Re/Os) having a modal gamma Os of around -1.

There are several additional isotopic signatures present in Harold's Grave chromitites. The lowest $^{187}Os/^{188}Os$ value recorded is 0.1183, found only in one composite interstitial PGM. This corresponds to a Re-depletion age of ~1400 Ma. A larger group of PGM (n=10) also have low $^{187}Os/^{188}Os$ ratios between 0.120 and 0.123, which may possibly comprise two distinct groups, one from 0.120 to ~0.121 (n=4), and another between 0.122 and 0.123 (n=6). The less radiogenic of these sub-groups corresponds to a Re-depletion age of 1000-1100 Ma. While it would be unwise to suggest any global significance to the existence of this group, from this dataset alone, it is interesting to note that this Grenvillian age has also been found in numerous larger datasets of detrital mantle-derived PGM: Urals, Tasmania (Pearson et al., 2007), Dongqiao Massif, Tibet (Shi et al., 2007) and the Rhine river (Dijkstra et al., 2016). In addition, some mantle peridotite datasets also contain a significant proportion of this signature, including abyssal peridotites (Brandon et al., 2000; Harvey et al., 2006) and Zealandia xenoliths (Liu et al., 2015; McCoy-West et al., 2013). These combined data have led to the suggestion that this is a widespread (global?) mantle depletion signature (Dijkstra et al., 2016; Pearson et al., 2007).

It has previously been noted, on a whole-rock scale, that distinct Shetland chromitite formations have differing Os isotope compositions (O'Driscoll et al., 2012). Here we note that these differences and also reflected in our limited data for PGM from Quoys and Cliff chromitites. The modal average $^{187}Os/^{188}Os$ ratio from Harold's Grave (~0.1245-0.1255) is absent from the five Quoys and Cliff PGM analysed, while the most common signature from Cliff and Quoys (~0.1272; four out of five PGM) is only found in one of 90 PGM analyses from Harold's Grave (Figure 17). This modal isotope composition for Cliff and Quoys reflects that those PGM have a more enriched source (or have been contaminated by crustal material), than almost all from Harold's Grave (85 out of 90 PGM).

The variable Os isotope signatures from individual PGM from within a single chromitite, and between chromitites, indicates heterogeneity of the Shetland chromitite mantle source in either space, time, or both, although it is unclear over what length- and time-scale such sources would

exist. Given the convergent margin origin of the Shetland ophiolite, it is plausible that different portions of mantle are sampled, both temporally and spatially, according to the dynamics of fluid fluxing and the corresponding partial melting.

## 5. CONCLUSIONS

X-ray computed tomography has been used to identify five distinct groups of PGM in the IPGE enriched chromitites from Harold's Grave in the Shetland ophiolite, of which two are predominant. Group (i) PGM consist almost exclusively of laurite sometimes accompanied by IPGE alloys, entirely enclosed within chromite grains. The Group (ii) PGM association occurs interstitial to chromite grains with a much greater diversity of PGM than in Group (i) including laurite, native Os, irarsite-hollingworthite and platarsite, sperrylite, (NiRhPtPd)Sb, PGE alloys and various PGE-oxides including Ru-oxide all accompanied by ruthenian pentlandite. Group (ii) accounts for the bulk of the total mass of PGMs in the samples. Group (iii) PGMs are elongate and aligned, comprise an assemblage of native Pt and native Os, Pt-Os alloy, IrSbS (possibly tolovkite), laurite, irarsite and a Pt-Rh-Ni-antimonide, and occur as multiple inclusions within particular individual chromite crystals only.

In contrast to the previous interpretation by Badanina et al. (2016), we do not regard the interstitial Group (ii) aggregates as being simply altered equivalents of the Group (i) assemblage, but rather as having a distinct petrogenesis. The Group (i) IPGE-rich laurites and alloys crystallised directly from the silicate parent magma and were engulfed in the chromite as it grew around them. Group (ii) interstitial aggregates are attributed to a two stage process involving initial collection by a sulfide liquid at very high R factor, followed by re-dissolution of this sulfide liquid into a later influx of sulfide-undersaturated magma. PGM containing IPGE, Pt and Rh are stabilised during the progressive reduction of sulfide liquid mass, and retained in the rock after the sulfide liquid has been completely re-dissolved. This process is closely akin to that postulated by Fonseca et al. (2012) to form Os-Ir alloys during mantle melting.

The general uniformity of $^{187}Os/^{188}Os$ ratios within the sample (67 of 90 PGM fall within uncertainty of 0.1245-0.1255) supports the contention of Badanina et al. (2016) that the Harold's Grave chromitites have behaved as a closed system for Re and Os at outcrop scale since the time of formation of the ophiolite. A small proportion of anomalously low, unradiogenic $^{187}Os/^{188}Os$ PGM with one at 0.1183, and 10 between 0.120 and 0.123. These ratios are probably a consequence of heterogeneities in the source of the parent magmas; specifically, long-term depleted sources. A smaller proportion of anomalously radiogenic samples ($^{187}Os/^{188}Os$ = 0.127-0.133; n = 5) attest to the rarer presence of melts from more enriched mantle sources. Regardless of the source, Os isotope heterogeneity is present among individual PGM, within a single hand specimen (cf. Marchesi et al., 2011), requiring that PGM form from discrete melts, sometimes with distinct sources.

Detailed petrographic observations suggest a complicated sequence of PGM crystallisation. The proposed model for the composite interstitial PGM aggregates involves a complex and probably unusual sequence of events, which is reflected in the extreme rarity of chromitites like Harold's Grave. However, the model of PGM formation by re-dissolution of sulfide may be a much more general hypothesis with applications to PGE geochemistry in a range of magma types and settings.

## 6. ACKNOWLEDGMENTS

We acknowledge a Distinguished Visiting Fellowship to Prof. Hazel Prichard CSIRO that made this work possible. The Os isotope analytical work in Durham was supported by a Natural Environment Research Council Grant NE/F005717/1. Steve Barnes is funded by the CSIRO Science Leader scheme. We thank Dr Duncan Muir for his help with the EBSD at Cardiff University We thank Dr Raul Fonseca, an anonymous reviewer and Prof. Ian Campbell for their careful consideration of the manuscript.

## 8. APPENDIX – analytical methods for Os isotopes

Osmium-bearing PGM were analysed for $^{187}Os/^{188}Os$ by laser ablation MC-ICPMS, using a New Wave UP 213 nm Nd:YAG laser system, coupled to a ThermoFinnigan Neptune MC-ICPMS at Durham Geochemistry Centre, Durham University. All isotopes of Os were analysed, together with the key elements which potentially cause isobaric interferences, $^{182}W$ and $^{185}Re$, in the configuration: $^{182}W$, $^{184}Os$, $^{185}Re$, $^{186}Os$, $^{187}Os$, $^{188}Os$, $^{189}Os$, $^{190}Os$, $^{192}Os$ in L4, L3, L2, L1, C, H1, H2, H3, H4 collectors, respectively. Due to the low Pt contents and relatively small size of the beams used, it was not necessary to omit $^{192}Os$ from the analytical procedure, although we did not use this isotope for the correction of mass bias, to avoid the potential effects of Pt interference on $^{192}Os$. Instead, a normalisation value of $^{189}Os/^{188}Os = 1.21978$ was used. Gain calibration, baselines, peak centring and peak shape were all measured and checked at the start of each analytical session, with greater detail given in Nowell et al. (2008a). Measurement consisted of 80 cycles each with 0.5-second integration time.

In total, Os isotopes were analysed over 11 analytical sessions, from May 2013 to September 2014, due to the need to polish down samples to expose new PGM. At the start of each session, a 1 ppm DROsS osmium standard solution was analysed at least five times to assess instrumental accuracy and reproducibility, and the laser ablation data were corrected for the offset of the DROsS values from the accepted value ($^{187}Os/^{188}Os = 0.160924$; Nowell et al., 2008a), although the correction was never more than 0.000015). Two variably doped 1 ppm DROsS solutions were also analysed to determine the factors required to correct for $^{184}W$, $^{186}W$ and $^{187}Re$ isobaric interferences during ablation analyses. These solutions, D1 and D2, had concentrations of W at 0.05 ppm and 0.1 ppm and Re at 0.01 and 0.05 ppm. Over the 11 sessions, the pure DROsS standards (n = 54) gave mean values of $^{187}Os/^{188}Os = 0.160919 \pm 16$ (2 s.d.), $^{186}Os/^{188}Os = 0.119917 \pm 09$ and $^{184}Os/^{188}Os = 0.001297 \pm 14$, equating to relative reproducibilities of 98 ppm, 73 ppm and 11 ‰, respectively. Overall, including the two doped solutions (n = 21 D1 and 15 D2) mean values were $^{187}Os/^{188}Os = 0.160920$, $^{186}Os/^{188}Os = 0.119917$ and $^{184}Os/^{188}Os = 0.001298$ with relative uncertainties of 99 ppm, 74 ppm and 11 ‰ (when corrected to $^{189}Os/^{188}Os = 1.21978$), in excellent agreement with published data of (Nowell et al., 2008a). The best fit $^{185}Re/^{187}Re$ and $^{182}W/^{186}W$, used for interference correction, varied over the course of the 11 sessions by 115 ppm and 143 ppm, respectively, with average values of 0.598156 and 0.929215. These variations are somewhat higher than the degree of uncertainty shown by DROsS values alone, but data from each analytical session was corrected with the corresponding values from that session. The additional issue that these values are determined from solutions (wet plasma), and thus are not strictly identical to those of laser ablation, is insignificant at the minor proportions that the interfering elements are present in the studied PGM

grains compared to those of the doped standards: $^{182}W/^{188}Os_{\text{Shetland PGM}}/^{182}W/^{188}Os_{\text{doped standard}}$ is always <0.023; while $^{185}Re/^{188}Os_{\text{Shetland PGM}}/^{185}Re/^{188}Os_{\text{doped standard}}$ is <0.06 for all PGM. Most importantly, the uncertainties for both the interference correction and the mean $^{187}Os/^{188}Os$ DROsS value are far smaller than the range of natural variation, which is ~85 ‰.

The methods for ablation and analysis closely followed those detailed in Nowell et al. (2008b), except that it was necessary to use smaller beam sizes of 12 to 30 µm, due to correspondingly small grain sizes. At the smaller beam sizes, the power of the laser beam was always kept to 90-100% to minimise any potential fractionation at the ablation site. Such fractionation is poorly understood and is mainly a consideration for inter-element fractionation, which is of secondary importance in this study because we use model age estimates rather than isochron dating methods. Nonetheless, we undertook additional tests to investigate potential effects of low overall laser energy and lower Os beam intensities (resulting from small laser spot sizes), compared to previous studies (Dijkstra et al., 2016; Nowell et al., 2008b). Tests on the Durham University in house standard, PGM sample 36720 from the Urals, show that uncorrected effects on $^{187}Os/^{188}Os$ and $^{186}Os/^{188}Os$ do exist when the $^{188}Os$ beam is less than 150 mV, due either to measurement effects or to lower overall laser power – the latter as a result of small laser spot sizes of 12 µm or less, or to lower laser power of ~60-80% on intermediate spot sizes of 20-30 µm. It has not been possible to completely deconvolve instrumental and laser power effects, but an instrumental effect is more likely due to the fact that $^{187}Os/^{188}Os$ (and $^{186}Os/^{188}Os$) ratios can deviate both above and below the accepted value for 36720 (Grain 2) of 0.12395 (measured on beam sizes of >4 V of $^{188}Os$; Nowell et al., 2008b). An error in the W or Re interference correction cannot account for the variation because both elements are present in similarly low proportions as in the Shetland PGM. The source of this variation, therefore, is probably variation in the baseline, despite an increased baseline measurement time of 30 seconds for these small beam analyses, although an unknown interference effect cannot be ruled out.

Regardless of the source, the tests indicate that when $^{187}Os/^{188}Os$ ratios deviate by more than 0.0008, then $^{184}Os/^{188}Os$ and $^{186}Os/^{188}Os$ also deviate such that these analyses are effectively filtered out by the thresholds outlined below. As $^{187}Os/^{188}Os$ deviations of less than 0.0008 are not always effectively screened out, the within run uncertainty on Shetland PGM analyses with $^{188}Os$ beams <150 mV has been combined with an uncertainty of 0.00066, which is 2 s.d. on the range of offsets from the true value for PGM 36720 for tests with equivalent beam sizes. A similar calculation of external precision has been done for larger beam sizes, with the following uncertainties from the 36720 tests: 0.00045 for $^{188}Os$ beams of 0.15 - 0.5 V, 0.00019 between 0.5 - 1 V, and 0.00007 for >1 V. While the resulting uncertainties are greater than many within-run uncertainties, they remain much smaller than the range observed between grains and relate to uncertainties in the Re-

depletion model ages ranging from 94 to 10 Ma for the range of beam sizes outlined – well within the overall uncertainty on model ages due to choice of reference and much less than the difference between groups of PGM identified in this study.

Mass bias and interfering element corrections were applied to each measurement, after which the analyses were subject to a 2σ rejection. The method and corrections are discussed in greater detail by Nowell et al. (2008b). The relatively high power and small grains resulted in complete destruction of some PGM, in which case some cycles were omitted due to low beam sizes, below 40 mV of $^{188}$Os. A number of filters were applied to the overall dataset to avoid potential inaccuracies as discussed above for the tests on PGM 36720. Average beam sizes below 40 mV $^{188}$Os were omitted due to the unreliability of ratios at this level, demonstrated for standard PGM 36720. Data were also required to fall (including 1 s.e. uncertainties) within the range of 0.0011 to 0.0015 for $^{184}$Os/$^{188}$Os (natural ratio: ~0.0013) and also above 0.119500 for $^{186}$Os/$^{188}$Os. While this threshold value for $^{186}$Os/$^{188}$Os is outside the range of permissible natural values (the solar system initial is ~0.119825; modern mantle is ~0.119835 (Brandon et al., 2000; Brandon et al., 2006)) this threshold ensures that no data reported deviates from the likely true value by more than 0.00035, even at 1 s.e. uncertainties. Such a deviation is insignificant compared to the natural variations observed in the $^{187}$Re - $^{187}$Os system (whole $^{187}$Os/$^{188}$Os range measured is 0.015, a factor of ~40 greater). Thus, any further filtering of the data is unnecessary for meaningful $^{187}$Os/$^{188}$Os comparison and has been avoided to ensure that the dataset was not skewed towards large PGM, which tend to be interstitial. Uncertainties on $^{184}$Os/$^{188}$Os and $^{186}$Os/$^{188}$Os were limited to 1 s.e. during filtering to ensure that imprecise data which deviated markedly from the true values were omitted. Correction for ingrowth of $^{187}$Os was insignificant, because no filtered PGM had $^{187}$Re/$^{188}$Os ratios greater than 0.031 (and only two of whole dataset were above this), but was performed nonetheless.

## REFERENCES


Ahmed A. H. and Arai S. (2003) Platinum-group minerals in podiform chromitites of the Oman ophiolite. *Can Min* **41**, 597–616.

Arai S., Prichard H. M., Matsumoto I. and Fisher P. C. (1999) Platinum-group minerals in podiform chromitite from the Kamuikotan zone, Hokkaido, northern Japan. *Res. Geol.* **49**, 39–47.

Augé T. (1986) Platinum-group mineral inclusions in chromitites from the Oman ophiolite. *Bull. de Minéral.* **109**, 301–304.

Augé T., Legendre O. and Maurizot P. (1998) The distribution of Pt and Ru-Os-Ir minerals in the New Caledonia ophiolite. In *International Platinum* (eds. N. P. Laverov and V. V. Distler). Athens, Theophrastus publications. pp. 141-154.

Badanina I. Y., Malitch K. N., Lord R. A., Belousova E. A. and Meisel T. C. (2016) Closed-system behaviour of the Re–Os isotope system recorded in primary and secondary platinum-group mineral assemblages: Evidence from a mantle chromitite at Harold's Grave (Shetland Ophiolite Complex, Scotland). *Ore Geol. Rev.* **75**, 174-185.

819 Bacuta G. C. J., Lipin B. R., Gibbs A. K. and Kay R.W. (1988) Platinum-group element abundance in
820 chromite deposits of the Acoje ophiolite block, Zambales ophiolite complex, Philippines. In
821 *Geo-Platinum Symposium Volume* (eds. H. M. Prichard,P. J. Potts, J. F. W. Bowles and S. J.
822 Cribb). Elsevier. pp. 381-382.
823 Ballhaus C., Bockrath C., Wohlgemuth-Ueberwasser C., Laurenz V. and Berndt J. (2006) Fractionation
824 of the noble metals by physical processes. *Contrib. Mineral. Petrol.* **152**, 667-684.
825 Barnes S. J. and Liu W. (2012) Pt and Pd mobility in hydrothermal fluids: evidence from komatiites
826 and from thermodynamic modelling. *Ore. Geol. Rev.* **44**, 49-58.
827 Barnes S .J., Fisher L. A., Godel B., Maier W.D., Paterson D., Howard D.L., Ryan C.G. and Laird J.S.
828 (2016) Primary cumulus platinum minerals in the Monts de Cristal Complex, Gabon: magmatic
829 microenvironments inferred from high-resolution x-ray fluorescence microscopy. *Contrib.*
830 *Mineral. Petrol.* **171**, 23-41.
831 Borisov, A. and Palme, H. (1995) Solubility of iridium in silicate melts: new data from experiments
832 with Ir10Pt90 alloys. Geochim. Cosmochim. Acta 59, 481-485.Borisov, A. and Palme, H. (2000)
833 Solubilities of noble metals in Fe-containing silicate melts as derived from experiments in Fe-
834 free systems. Amer. Mineral. **85**, 1665- 1673.
835 Borisov, A. and Walker, R.J. (2000) Os solubility in silicate melts: New efforts and results. Amer.
836 Mineral. 85, 912- 917.
837 Brandon, A.D., Snow, J.E., Walker, R.J., Morgan, J.W. and Mock, T.D. (2000) 190Pt-186Os and 187Re-
838 187Os systematics of abyssal peridotites. Earth and Planetary Science Letters **177**, 319-335.
839 Brandon, A.D., Walker, R.J. and Puchtel, I.S. (2006) Platinum-Osmium Isotope Evolution of the
840 Earth's Mantle: Constraints From Chondrites and Os-Rich Alloys. Geochimica Et Cosmochimica
841 Acta **70**, 2093-2103.
842 Brenan, J.M. (2002) Re-Os fractionation in magmatic sulfide melt by monosulfide solid solution.
843 Earth Planet. Sci Letts. **199**, 257- 268.
844 Brenan J.M. and Andrews D. (2001) High-temperature stability of laurite and Ru–Os–Ir alloy and
845 their role in PGE fractionation in mafic magmas. *Can Mineral* **39**, 341-360.
846 Brenan, J.M, Finnigan, C.S., McDonough, W.F., Homolova, V. (2012) Experimental constraints on the
847 partitioning of Ru, Rh, Ir, Pt and Pd between chromite and silicate melt; the importance of
848 ferric iron. Chemical Geology, **302-303**, p.16-32
849 Brenan, J.M., McDonough, W.F. and Ash, R. (2005) An experimental study of the solubility and
850 partitioning of iridium, osmium and gold between olivine and silicate melt. Earth Planet. Sci
851 Letts. **237**, 855-872.
852 Brenan, J.M. and Rose, L.A. (2002) Experimental constraints on the wetting of chromite by sulfide
853 liquid. Canadian Mineralogist **40**, 1113-1126.
854 Bridges J. C., Prichard H. M., Neary C. R. and Meireles C. A. (1993) Platinum-group element
855 mineralization in the chromite-rich rocks of the Braganca massif, northern Portugal. *Trans Inst.*
856 *Min. and Metall B* **102**, 103-113.
857 Brough C. P., Prichard H. M**.,** Neary C. R., Fisher P. C. and McDonald, I (2015) Geochemical variations
858 within podiform chromitite deposits in the Shetland Ophiolite: Implications for petrogenesis
859 and PGE concentration. *Econ. Geol.* **110**, 187–208
860 Campbell I. H. and Naldrett A. J. (1979) The influence of silicate:sulfide ratios on the geochemistry
861 of magmatic sulfides. *Econ. Geol.* **74**, 1503-1506.
862 Constantinides C. C., Kingston G. A. and Fisher P. C. (1980) The occurrence of platinum-group
863 minerals in chromitites of the Kokkinorostos chrome mine, Cyprus. In *International Ophiolite*
864 *Symposium Volume* (ed. A. Panayiotou). Geological Survey of Cyprus. pp. 93–101.
865 Corrivaux L. and Laflamme J. H. G.( 1990) Minéralogie des éléments du groupe du platine dans les
866 chromitites de l'ophiolite de Thetford mines, Québec. Can Mineral. **28**, 579-595.
867 Derbyshire, E.J., O'Driscoll, B., Lenaz, D., Gertisser, R. and Kronz, A. (2013) Compositionally
868 heterogeneous podiform chromitite in the Shetland ophiolite complex (Scotland); implications

for chromitite petrogenesis and late stage alteration in the upper mantle portion of a supra-subduction zone ophiolite. Lithos **162-163**, 279-300.

Dijkstra, A.H., Dale, C.W., Oberthür, T., Nowell, G.M. and Pearson, D.G. (2016) Osmium isotope compositions of detrital Os-rich alloys from the Rhine River provide evidence for a global late Mesoproterozoic mantle depletion event. Earth and Planetary Science Letters **452**, 115-122.

Economou-Ellopoulos M. (1996) Platinum-group element distribution in chromite ores from ophiolite complexes: Implications for their exploration. *Ore Geol, Rev.* **11**, 363–381.

Finnigan C. S., Brenan J. M., Mungall J. E. and McDonough W. F. (2008) Experiments and models bearing on the role of chromite as a collector of platinum-group minerals by local reduction. Jl Pet. **49**, 1647-1665.

Flinn D. (1985) The Caledonides of Shetland. In *The Caledonide Orogeny - Scandinavia and related Areas* (eds. D. G. Gee and B. A. Sturt). John Wiley and Sons Ltd. pp. 1159-1172.

Flinn D. and Oglethorpe J. D. (2005) A history of the Shetland Ophiolite Complex. Scot. Jl. Geol. **41**, 141-148.

Fonseca R. O. C., Campbell I. H., O'Neill H. S. C. and Allen C. M. (2009) Solubility of Pt in sulphide mattes: Implications for the genesis of PGE-rich horizons in layered intrusions. *Geochim. Cosmochim. Acta* **73,** 5764-5777.

Fonseca R. O. C., Laurenz V., Mallmann G., Luguet A., Hoehne N. and Jochum K. P. (2012) New constraints on the genesis and long-term stability of Os-rich alloys in the Earth's mantle. *Geochim. Cosmochim. Acta* **87**, 227-242.

Genkin A. D., Laputina I. P. and Mivavitskaya G. M. (1974) Ruthenium and rhodium-containing pentlandite - an indicator of hydrothermal mobilization of platinum minerals. *Geol. Rudnykl Mestaroz.***6**, 102-106 (translation 1976, *Internat. Geol. Rev*. **18**, 723-728).

Godel B. (2013) High-Resolution X-Ray Computed Tomography and Its Application to Ore Deposits: From Data Acquisition to Quantitative Three-Dimensional Measurements with Case Studies from Ni-Cu-PGE Deposits. *Econ. Geol.* **108**, 2005-2019.

Godel, B. M., Barnes, S. J., Barnes, S.-J., Maier, W. D. (2010). Platinum ore in 3D: Insights from high-resolution X-ray computed tomography. *Geology* **38**, 1127-1130.

Godel, B., Rudashevsky, N. S., Nielsen, T. F. D., Barnes, S. J., Rudashevsky, V. N. (2014). New constraints on the origin of the Skaergaard Intrusion Cu-Pd-Au mineralization: Insights from high-resolution X-ray computed tomography. *Lithos* **190-191**, 27-36.

González-Jiménez J. M., Griffin W. L., Proenza A., Gervilla F., O'Reilly S. Y., Akbulut M., Pearson N. J. and Arai S. (2014) Chromitites in ophiolites: How, where, when, why? Part II. The crystallisation of chromitites. *Lithos* **190-191**, 140-158.

Griffin W. L., Spetsius Z. V., Pearson N. J., and O'Reilly S. Y. (2002) *In situ* Re-Os analysis of sulfide inclusions in kimberlitic olivine: New constraints on depletion events in the Siberian lithospheric mantle. *Geochem. Geophys. Geosystems* **3**, 1-25.

Harvey, J., Gannoun, A., Burton, K.W., Rogers, N.W., Alard, O. and Parkinson, I.J. (2006) Ancient melt extraction from the oceanic upper mantle revealed by Re-Os isotopes in abyssal peridotites from the Mid-Atlantic ridge. Earth and Planetary Science Letters **244**, 606-621.

Kerr A. and Leitch A. M. (2005) Self-Destructive Sulfide Segregation Systems and the Formation of High-Grade Magmatic Ore Deposits. *Econ. Geol.* **100**, 311-332.

Kozul H., Prichard H. M., Melcher F., Fisher P. C., Brough C. and Stueben D.(2014) Platinum group element (PGE) mineralisation and chromite geochemistry in the Berit ophiolite (Elbistan/Kahramanmaraş), SE Turkey. *Ore Geol. Rev*. **60**, 97–111.

Liu J., Scott J. M., Martin C. E. and Pearson D. G. (2015). The longevity of Archean mantle residues in the convecting upper mantle and their role in young continent formation. *Earth. Planet. Sci. Lett.* **424**, 109-118.

Ludwig, K.R. (2003) User's manual for Isoplot 3.00: a geochronological toolkit for Microsoft Excel. Kenneth R. Ludwig.

Marchesi, C., Gonzalez-Jimenez, J.M., Gervilla, F., Garrido, C.J., Griffin, W.L., O'Reilly, S.Y., Proenza, J.A. and Pearson, N.J. (2011) In situ Re-Os isotopic analysis of platinum-group minerals from the Mayari-Cristal ophiolitic massif (Mayari-Baracoa Ophiolitic Belt, eastern Cuba): implications for the origin of Os-isotope heterogeneities in podiform chromitites. Contrib. Mineral. Petrol. **161**, 977-990.

McCoy-West, A.J., Bennett, V.C., Puchtel, I.S. and Walker, R.J. (2013) Extreme persistence of cratonic lithosphere in the southwest Pacific: Paleoproterozoic Os isotopic signatures in Zealandia. Geology **41**, 231-234.

Meisel, T., Walker, R.J., Irving, A.J. and Lorand, J.P. (2001) Osmium isotopic compositions of mantle xenoliths: A global perspective. Geochimica et Cosmochimica Acta **65**, 1311-1323.

Mungall, J.E. (2014) Geochemistry of Magmatic Ore Deposits, in: Holland, H.D., Turekian, K.K. (Eds.), Treatise on Geochemistry (Second Edition). Elsevier, Oxford, pp. 195-218.

Mungall J. E. and Brenan, J. M. (2014) Partitioning of the platinum-group elements and Au between sulfide liquid and basalt and the origins of mantle-crust fractionation of the chalcophile elements: Geochim. Cosmochim. Acta **125**, 265-289.

Naldrett A. J. (2004) *Magmatic Sulfide Deposits: Geology, Geochemistry and Exploration*. Springer, Heidelberg.

Naldrett, A.J., Lehmann, J. and Auge, T. (1989) Spinel non-stoichiometry and reactions between chromite and closely associated sulphides, with examples from ophiolite complexes, in: Prendergast, M.D., Jones, M.J. (Eds.), Magmatic sulphides - Zimbabwe Volume. Inst. Min. and Metall., London, pp. 221-228.

Naldrett, A.J., Kinnaird, J.A., Wilson, A., Yudovskaya, M.A., McQuade, S., Chunnett, G., and Stanley, C., 2009, Chromite composition and PGE content of Bushveld chromitites: Part 1 - the Lower and Middle Groups: Transactions of the Institute Mining and Metallurgy, B, v. 118, p. 131-161.

Nowell, G.M., Luguet, A., Pearson, D.G. and Horstwood, M.S.A. (2008a) Precise and accurate 186Os/188Os and 187Os/188Os measurements by multi-collector plasma ionisation mass spectrometry (MC-ICP-MS) part I: Solution analyses. Chemical Geology **248**, 363-393.

Nowell, G.M., Pearson, D.G., Parman, S.W., Luguet, A. and Hanski, E. (2008b) Precise and accurate 186Os/188Os and 187Os/188Os measurements by Multi-collector Plasma Ionisation Mass Spectrometry, part II: Laser ablation and its application to single-grain Pt-Os and Re-Os geochronology. Chemical Geology **248**, 394-426.

O'Driscoll B., Day J. M. D., Walker R. J., Daly J. S., McDonough W. F. and Piccoli P. M. (2012) Chemical heterogeneity in the upper mantle recorded by peridotites and chromitites from the Shetland Ophiolite Complex, Scotland. *Earth. Planet. Sci. Lett.* **333-334**, 226-237.

Ohnenstetter M., Johan Z., Coherie A., Fouillac A., Guerrot C., Ohnenstetter D., Chaussidon M., Rouer O., Makovicky E., Makovicky M., Rose-Hansen J., Karup-Moller S., Vaughan D., Tumer G., Pattrick R. A. D., Gize A.P., Lyon I. and McDonald I. (1999) New exploration methods for platinum and rhodium deposits poor in base-metal sulfides. *Trans Inst. Min. Metall. B,* **108**, 119-150.

Orberger B., Fredrich G. and Woermann E. (1988) Platinum-group element mineralisation in the ultramafic sequence of the Acoje ophiolite block, Zambales, Philippines. In *Geo-Platinum Symposium Volume* (eds. H. M. Prichard,P. J. Potts, J. F. W. Bowles and S. J. Cribb). Elsevier. pp. 361-380.

Page N. J. and Talkington R W. (1984) Palladium, platinum, rhodium, ruthenium, and iridium in peridotites and chromitites from ophiolite complexes in Newfoundland. *Can. Mineral.* **22**, 137–149.

Page N., Cassard D. and Haffty J. (1982) Palladium, platinum, rhodium, ruthenium, and iridium in chromitites from the Massif du Sud and Tiebaghi Massif, New Caledonia. *Econ. Geol.* **77**, 1571–1577.

Pagé P and Barnes S-J. (2013) Improved in-situ determination of PGE concentration of chromite by LA-ICP-MS: Towards a better understanding. *Mineral Deposit research for a high tech world, 12th Biennial SGA Meeting,* Uppsala. #1050-1053 (abstr.).

Pagé P. and Barnes S-J. (2016) The influence of chromite on osmium, iridium, ruthenium and rhodium distribution during early magmatic processes. *Chem. Geol.* **420**, 51-68.

Pagé, P., Barnes, S.-J., Bedard, J.H. and Zientek, M.L. (2012) In situ determination of Os, Ir, and Ru in chromites formed from komatiite, tholeiite and boninite magmas; implications for chromite control of Os, Ir and Ru during partial melting and crystal fractionation. Chem. Geol. **302-303**, 3-15.

Park J-W., Campbell I. H. and Eggins S. M. (2012) Enrichment of Rh, Ru, Ir and Os in Cr spinels from oxidized magmas: evidence from the Ambae volcano, Vanuatu. *Geochim Cosmochim Acta* **78**, 28-50.

Pearson, D.G., Parman, S.W. and Nowell, G.M. (2007) A link between large mantle melting events and continent growth seen in osmium isotopes. Nature **449**, 202-205.

Pearson N. J., Alard O., Griffin W. L., Jackson S. E., and O'Reilly S. Y. (2002) *In situ* measurement of Re-Os isotopes in mantle sulfides by laser ablation multicollector-inductively coupled plasma mass spectrometry: analytical methods and preliminary results. *Geochim Cosmochim. Acta **66***, 1037-1050.

Pedersen R.B., Johannesen G.M. and Boyd, R. (1993) Stratiform PGE mineralisations in the ultramafic cumulates of the Leka ophiolite complex, central Norway. *Econ. Geol.* **88**, 782-803.

Peregoedova, A., Barnes, S. J., and Baker, D. R., 2004, The Formation of Pt-Ir Alloys and Cu-Pd-Rich Sulfide Melts by Partial Desulfurization of Fe-Ni-Cu Sulfides: Results of Experiments and Implications for Natural Systems: Chemical Geology, v. 208, p. 247-264.

Prichard H. M. (1985) The Shetland Ophiolite, In *The Caledonide Orogeny - Scandinavia and related Areas* (eds. D. G. Gee and B. A. Sturt). John Wiley and Sons Ltd. pp. 1173-1184.

Prichard H. M. and Brough, C.P. (2009) Potential of ophiolite complexes to host PGE deposits. In *New Developments in magmatic Ni-Cu and PGE deposits* (eds. C. Li and E. M. Ripley). Beijing, Geological Publishing House. pp. 277 - 290.

Prichard H. M. and Lord, R.A. (1988) The Shetland ophiolite: Evidence for a supra-subduction origin and implications for PGE mineralization. In *Mineral Deposits in the European Community* (eds. J. Boissonnas and P. Omenetto). Springer Verlag. pp. 289-302.

_____ (1990) Platinum and palladium in the Troodos ophiolite complex, Cyprus. *Can. Mineral.* **28**, 607–617.

_____ (1993) An overview of the PGE concentrations in the Shetland ophiolite complex. In *Magmatic Processes and Plate Tectonics* (eds. H. M. Prichard, T. Alabaster, N. B. Harris and C. R. Neary). Volume 76, Geological Society of London.p p. 273-294.

Prichard H. M., and Tarkian M. (1988) Platinum and palladium minerals from two PGE-rich localities in the Shetland Ophiolite Complex. *Can. Mineral.* **26**, 979-990.

Prichard, H.M., Barnes, S.J. and Godel, B., 2017. A mechanism for chromite growth in ophiolite complexes: Evidence from 3d high-resolution x-ray computed tomography images of chromite grains in Harold's Grave chromitite in the Shetland ophiolite. Mineralogical Magazine, accepted.

Prichard H. M., Economou-Eliopoulos M. and Fisher P. C. (2008b) Platinum-group minerals in podiform chromitite in the Pindos ophiolite complex, Greece. *Can. Mineral.* **46**, 329 - 341.

Prichard H. M., Ixer R. A., Lord R. A., Maynard J. and Williams N. (1994) Assemblages of platinum-group minerals and sulfides in silicate lithologies and chromite-rich rocks within the Shetland Ophiolite. *Can. Mineral.* **32**, 271-294.

Prichard, H.M., Lord, R.A. and Neary, C.R. (1996) A model to explain the occurrence of platinum- and palladium-rich ophiolite complexes. J. Geol. Soc. London 153, Part 2, 323-328.

Prichard H. M., Neary C. R., Fisher P. C. and O'Hara M. J. (2008a) PGE-rich podiform chromitites in the Al'Ays Ophiolite complex, Saudi Arabia: An example of critical mantle melting to extract and concentrate PGE. *Econ. Geol.* **103**, 1507-1529.

Prichard H. M., Neary C. R. and Potts P.J. (1986) Platinum-group minerals in the Shetland Ophiolite. In Metallogeny of the Basic and Ultrabasic Rocks (eds. M. J. Gallagher, R. A. Ixer,C. R. Neary and H. M. Prichard). Inst. Min. Metall.pp. 395-414.

Righter, K., Campbell, A.J., Humayun, M. and Hervig, R.L. (2004) Partitioning of Ru, Rh, Pd, Re, Ir and Au between Cr-bearing spinel, olivine, pyroxene and silicate melts. Geochimica et Cosmochimica Acta 68, 867-880.

Shi, R.D., Alard, O., Zhi, X.C., O'Reilly, S.Y., Pearson, N.J., Griffin, W.L., Zhang, M. and Chen, X.M. (2007) Multiple events in the Neo-Tethyan oceanic upper mantle: Evidence from Ru-Os-Ir alloys in the Luobusa and Dongqiao ophiolitic podiform chromitites, Tibet. Earth and Planetary Science Letters **261**, 33-48.

Shirey S. B. and Walker R. J. (1998) The Re-Os isotope system in cosmochemistry and high-temperature geochemistry. *An. Rev. Earth. Planet. Sci.* **26**, 423-500.

Silverman, B.W. (1986) Density estimation for statistics and data analysis. CRC press.

Spray, J.G., Dunning, G.R., 1991. A U/Pb age for the Shetland Islands oceanic fragment, Scottish Caledonides: evidence from anatectic plagiogranites in 'layer 3' shear zones. Geological Magazine 128, 667-671.

Tarkian M. and Prichard H. M. (1987) Irarsite-Hollingworthite Solid-Solution Series and Other Associated Ru-, Os-, Ir-, and Rh bearing PGM's from the Shetland Ophiolite Complex. *Min. Dep.* **22**, 178-184.

Walker, R.J., Horan, M.F., Morgan, J.W., Becker, H., Grossman, J.N. and Rubin, A.E. (2002a) Comparative Re-187-Os-187 systematics of chondrites: Implications regarding early solar system processes. Geochimica et Cosmochimica Acta 66, 4187-4201.

Walker, R.J., Prichard, H.M., Ishiwatari, A. and Pimentel, M. (2002b) The osmium isotopic composition of convecting upper mantle deduced from ophiolite chromites. Geochimica et Cosmochimica Acta **66**, 329-345.

Xiong, y. Hydrothermal transport and deposition of Rhenium under subcriticval conditions revisited. Economic Geology 101, 471-478.

Zhou M-F., Robinson P.T., Malpas J. and Li Z. (1996) Podiform Chromitites in the Luobusa Ophiolite (Southern Tibet): Implications for Melt-Rock Interaction and Chromite Segregation in the Upper Mantle. *Jl Pet.* **37**, 3-21.

# Figure Captions

Figure 1. Map of the Shetland ophiolite (diagram adapted from Brough et al. 2014).

Figure 2. A) to F) 3D computed tomography images of PGM in sample HG6 (PGM in blue) and sample HG6A (PGM in red) showing individual laurite (round) and composite laurite and IPGE alloys (elongate and angular). A) and B) are composite grains, C) shows a laurite attached to a silicate inclusion (black) in the chromite which is not in contact with any external silicate, E) and F) are laurites not associated with elongate Os-Ir alloys. The images show that the individual PGM and the one PGM attached to a silicate inclusion are entirely enclosed in chromite; an observation that can only be confirmed in a 3D image. G) PGM in HG6A shown within the two 3D computed tomography partially imaged chromite grains (outlined in black and separated by serpentine in pale green), and H) a close up of part of one of these grains shown by a box on G) revealing that the locations of PGM (red and circled in red) are approximately evenly distributed and predominantly located away from silicate equant shaped silicate inclusions (dark grey and blue) and silicate filled fractures (blue) that cross the chromite grain.

Figure 3. Abundance of types of PGM enclosed in the chromite grains belonging to Group (i) (enclosed in chromite grains – A and B) and Group (ii) PGE-bearing minerals interstitial to the chromite grains in HG6 (C and D), A and C) classification by numbers of PGM grains observed and B and D) by sectional area.

Figure 4. Back scattered scanning electron microscope images of polished thin sections of typical examples of laurites (Lrt) and associated PGM alloys and silicate inclusions (dark grey or black) located within chromite grains in HG6. B) and G) are composite grains of laurite, Os-Ir-Ru alloy and very small Pt-bearing PGM.

Fig. 5 A-C. Group (ii) PGM are defined as those located interstitial to the chromite grains. Some large composite PGM appear to be enclosed in chromite grains but EBSD reveals that the chromite grains are often divided into groups of grains. A) A composite PGM belonging to group (ii) that appears to be enclosed in a chromite grain shown in B). The PGM is marked by a white circle. C) EBSD image of the chromite grain containing the PGM. The area of the EBSD analysis is marked by a white rectangle shown in B). The EBSD image shows that the chromite grain is composed of several chromite grains, with different orientations indicated by different colours, and the PGM cluster is at the junction of two of these grains. D-I, Typical examples of PGM located interstitial to chromite grains in HG6 observed as a back scattered SEM image in polished thin section. D) composite grain of laurite, enclosing grains of irarsite and many smaller grains of native Os, E) laurite rimed by Os-rich laurite, F) a composite grain of laurite rimed by Os-rich laurite containing abundant small grains of native Os,

1084 all attached to irarsite rimed by hollingworthite and a Pt-Fe alloy, and associated with a Ru-oxide
1085 that is located adjacent to the laurite, G) sperrylite ($PtAs_2$), H) a Rh-Ni-Pt-antimonide and
1086 sulpharsenides associated with heazlewoodite and digenite and I) composite grain of laurite with
1087 irarsite and heazlewoodite enclosing native Os.

1088 Figure 6. Computed tomography 3D image of HG6 showing a circular slice of chromitite with
1089 chromite grains shown in grey, silicate in black and PGM in blue. A) view looking at the image
1090 oriented with the long axis of the sample core at right angles to the plane of view and B) view at
1091 right angles to A). The large PGM is shown in Figure 10. C) view of the entire largest PGM grain and
1092 associated smaller grains of ruthenian pentlandite and Pt-Rh-Sb, (all white) interstitial to chromite
1093 grains (grey) and surrounded by silicate (black), D)Close up of the large grain showing that it is a
1094 composite grain of ruthenian pentlandite, laurite, irarsite and many tiny grains of native Os, E) close
1095 up of area outlined by a box in D) showing irarsite labelled 1 and 2 with 2 containing more Rh and 3
1096 hollingworthite (analyses at locations 1-3 given in Table 5) surrounded by laurite and ruthenian
1097 pentlandite both hosting native Os. Abbreviations used:- Lrt - laurite, (Ru-Pn) = ruthenian
1098 pentlandite, Os = native Osmium.

1099 Figure 7. 3D computed tomography image of HG1 showing PGM (red) above a view of a circular
1100 basal slice through the core of chromitite with chromite (black) and interstitial silicate (blue). A) all of
1101 the PGM imaged in red. B) close-up of the aligned PGM ringed in A) and coloured blue in Figure 13.
1102 They occur in one chromite grain shown below the PGM with the lowest PGM just visible above the
1103 grain.

1104 Fig 8. Osmium isotope frequency plots – distribution of $^{187}Os/^{188}Os$ and corresponding Re depletion
1105 ($T_{RD}$) ages in Os-rich mono-mineralic or composite PGM grains from Harold's Grave. A, all
1106 measurements; B, grains entirely enclosed in chromite; C, grains or clusters within interstitial silicate,
1107 or with indeterminate relationships to chromite. Any duplicate analyses were excluded (hence 83
1108 analyses in total). The curves were calculated using Isoplot (Ludwig, 2003). A uniform 'bandwith'
1109 uncertainty of 0.0005 was used, which is slightly larger than the optimal bandwidths (0.0003 to
1110 0.0004) according to Silverman's rule of thumb (Silverman, 1986). The increased bandwidth was
1111 used to limit exaggeration of peaks produced by small numbers of isotopically distinct grains. The
1112 histograms provide an alternative representation.

1113 Figure 9. Model of PGM formation, A) laurite and Os-Ir-Ru alloys crystallise as the chromite
1114 crystallises, group (i), group (iii) also crystallise in a few chromite grains, B) remaining PGE are
1115 collected by immiscible sulphide droplets that collect interstitially to the chromite grains with
1116 silicates, C) sulfides dissolve into a passing PGE-undersaturated silicate magma while laurite

continues to crystallise, D) further S loss to the silicate magma results in Os-Ir alloys forming, E) further S loss allows Pt PGM to form close to the point of final dissolution of sulfide, while some laurite reacts with the sulfide liquid to form Ru-pentlandite as Pd and Cu dissolve into the silicate magma as all remaining sulfide liquid dissolves, F) PGM alter as As is introduced on emplacement of the ophiolite; local shearing of chromite deforms PGM, G). Evolution of PGE contents of sulfide melt, assuming initial formation from a boninite-like parent magma at high R value, followed by progressive increase of PGE tenor as sulfide dissolves, to the point of saturation in Os-Ir phases after ~50% dissolution, and Pt PGM phase(s) close to final sulfide disappearance point.

Electronic supplementary material

Figures/images:

Figure S1 was 8 Abundance of PGM enclosed in chromite or interstitial to the chromite and for HG1 abundance of elongate and oriented PGM enclosed in chromite. A) number of PGM in HG6, B) area of PGM in HG6, C) number of PGM in HG1 and HG 8, D) area of PGM in HG 1 and 8 and E) areas of PGM in the interstitial cluster in HG 7.

Figure S2 was 10. 3D computed tomography images of a cluster of PGM present in HG7, A) image showing the distribution of PGM in the whole of the core imaged, B) close up of the cluster or group of PGM located in HG7 showing the PGM (red) and the ruthenian pentlandite (pale green) with a slice of chromitite below and in the background showing chromite grains (light grey) and interstitial silicate (dark grey) and C) rotated image of the same cluster shown in B) revealing how the PGM form an 'S' shape caused by the PGM being wrapped around two chromite grains (whose edges are outlined in white) . Vertical height of cluster = approx. 0.9 mm.

Figure S3 was 11. Relative abundance/area of IPGE-bearing minerals in the cluster of PGM in HG7 A) plotted by area of IPGE-bearing minerals observed and B) also by area with the exclusion of the two most abundant PGE-bearing minerals which are ruthenian pentlandite and irarsite (Shown in A).

Fig. S4 was 14. PGM located in a co-planar array that traverses a layer of chromitite probably filling an annealed fracture. A, B) Perspective view of a 3D tomography image of a microcore showing PGM. A), chromite in blue, silicates in red. B) same volume, with PGM shown in red. Note coplanar array, ringed, C, perspective view showing orthogonal planes through the image (chromite darker grey, silicate lighter) with one of these planes arranged parallel o the planar array of PGMs. D) and E) are large laurites forming part of the planar array.

Figure S5 was 15. 3D computed tomography image of chromitite in sample HG6A showing two phases of shearing of the PGM within narrow shear zones cross cutting the sample. A) section of HG6A showing a grain of chromite with serpentine filled undeformed pull-apart textures (p, two sub-vertical features centre and far right, shown in blue and black), silicate inclusions (i, shown as equant dark areas) and a cross cutting shear (s, picked out by parallel rows of dark dots crossing the entire area from bottom right to top left). D (deformed) and E (undeformed) PGM in the shear zone and away from the shear zone respectively (red). B) another area of sheared PGM (red) shown as two clusters (1 and 2) in the shear zone which is marked by a line of serpentine S that is picked out in dark grey as it crosses the chromite grain (light grey) shown in a computed tomography imaged slice below the PGM. The larger cluster forms a row of PGM that have been broken up and aligned within the plane of the shear. C) Close up of the larger cluster of PGM (1) showing that it has been sheared into a line and then sheared again deforming individual PGM in a second direction (shown as sub-horizontal). Shear directions indicated by black arrows. D) sheared PGM, E) unsheared PGM that is not in the shear zone and F) photomicrograph of a sheared PGM as viewed in 2D in a polished block in sample Q3 from Harold's Grave.

Fig. S6 was 17. Composite Os-bearing PGM, that have low $^{187}Os/^{188}Os$ ratios, all from Harold's Grave. Pairs of back scattered scanning electron microscope photomicrographs showing details of the composite PGM at high magnification and textural sites of the PGM in chromite at low magnification, Lrt = laurite, Ru-pn = ruthenian pentlandite, Chr = chromite and Si = altered silicate, mainly serpentine but with some Cr-chlorite, A) to L) have ages that correspond to ~1150 Ma and M) and N) have an age corresponding to ~1400 Ma. Os isotope data as follows: A) and B) HG3 $^{187}Os/^{188}Os$ 0.1208; C) and D) HG5 $^{187}Os/^{188}Os$ 0.12191; E) and F) HG10 $^{187}Os/^{188}Os$ 0.1205; G) and H) HG4 $^{187}Os/^{188}Os$ 0.1220; I) and J) HG1 $^{187}Os/^{188}Os$ 0.1211; K) and L) HG7 $^{187}Os/^{188}Os$ 0.1211; M) and N) HG4 $^{187}Os/^{188}Os$ 0.1183.

Fig. S7 was 18. Composite Os-bearing PGM, from podiform chromitite in the mantle harzburgite in other sites than Harold's Grave, A) and B), Cliff C)-F) and Quoys G)-L). Pairs of back scattered scanning electron microscope photomicrographs showing details of the composite PGM at high magnification and textural sites of the PGM in chromite at low magnification, Lrt = laurite, Ru-pn = ruthenian pentlandite, Chr = chromite and Si = altered silicate, mainly serpentine but with some Cr-chlorite, ages correspond to those of the ophiolite or slightly younger. Os isotope data as follows: A)and B) Nikkavord South $^{187}Os/^{188}Os$ of ~0.1266 (but data rejected due to low $^{186}Os/^{188}Os$ ratio), C)and D) Cliff $^{187}Os/^{188}Os$ 0.1300, E)and F) Cliff $^{187}Os/^{188}Os$ 0.12721, G)and H) Quoys $^{187}Os/^{188}Os$ s 0.12708, I)and J) Quoys $^{187}Os/^{188}Os$ 0.12723, K)and L) Quoys $^{187}Os/^{188}Os$ 0.12720.

**SUPPLEMENTARY MATERIAL – Data Tables**

Table S1 – size and spatial resolution data on samples analysed by HRXCT

Table S2 - Semi-quantitative SEM analyses of laurite and IPGE alloys enclosed within chromite grains.

Table S3 - Quantitative analyses of PGM external to chromite grains

Table S4 - Table of complete Os isotope data (Excel file)

Table 1. PGE analyses of chromitites examined in this study (From Brough et al. 2014).

| **Sample Number** | **Pt** | **Pd** | **Rh** | **Os** | **Ir** | **Ru** | **Total PGE** |
|---|---|---|---|---|---|---|---|
| | ppb | ppb | ppb | ppb | ppb | ppb | ppb |
| HG1 | 474 | 40 | 349 | 1647 | 2040 | 3400 | 7950 |
| HG6 | 566 | 40 | 422 | 2968 | 2861 | 7311 | 14168 |
| HG7 | 785 | 69 | 397 | 1324 | 2270 | 3483 | 8328 |
| HG8 | 685 | 36 | 344 | 1479 | 2088 | 3183 | 7815 |

Table 2. PGM imaged in the 5 samples analysed in 3D. HG8 is less massive chromitite than the other samples.

| Sample No. | No. Of PGM imaged | Largest Microns Length | PGM Width | Smallest Microns Length | PGM Width |
|---|---|---|---|---|---|
| HG6A | 51 | 22 | 15 | 1.4 | 0.7 |
| HG6 | 17 | 199 | 121 | 3.4 | 3.4 |
| HG1 | 74 | 293 | 224 | 19.8 | 19.8 |
| HG7 | 46 | 644 | 220 | 19.8 | 14.0 |
| HG8 | 7 | 222 | 158 | 19.8 | 19.8 |

Table 3 Numbers and areas of PGM analysed in HG6 separated into interstitial and enclosed by chromite

| | Interstitial | | Enclosed | |
|---|---|---|---|---|
| | No. PGM | Area PGM | No. PGM | Area PGM |
| Laurite | 17 | 10580 | 9 | 221 |
| IrAsS | 35 | 1231 | | |
| Ru pent | 13 | 1182 | | |
| Native Os | 115 | 490 | | |
| (NiRhPt)Sb | 7 | 52 | | |
| RhIrAsS | 3 | 43 | | |
| PtFe | 3 | 42 | 1 | 0.25 |
| RuO | 1 | 32 | | |
| PtAs | 2 | 24 | | |
| OsIr alloy | 5 | 6 | 6 | 53 |
| PtIrAs | 2 | 1 | | |

**Figure 1**

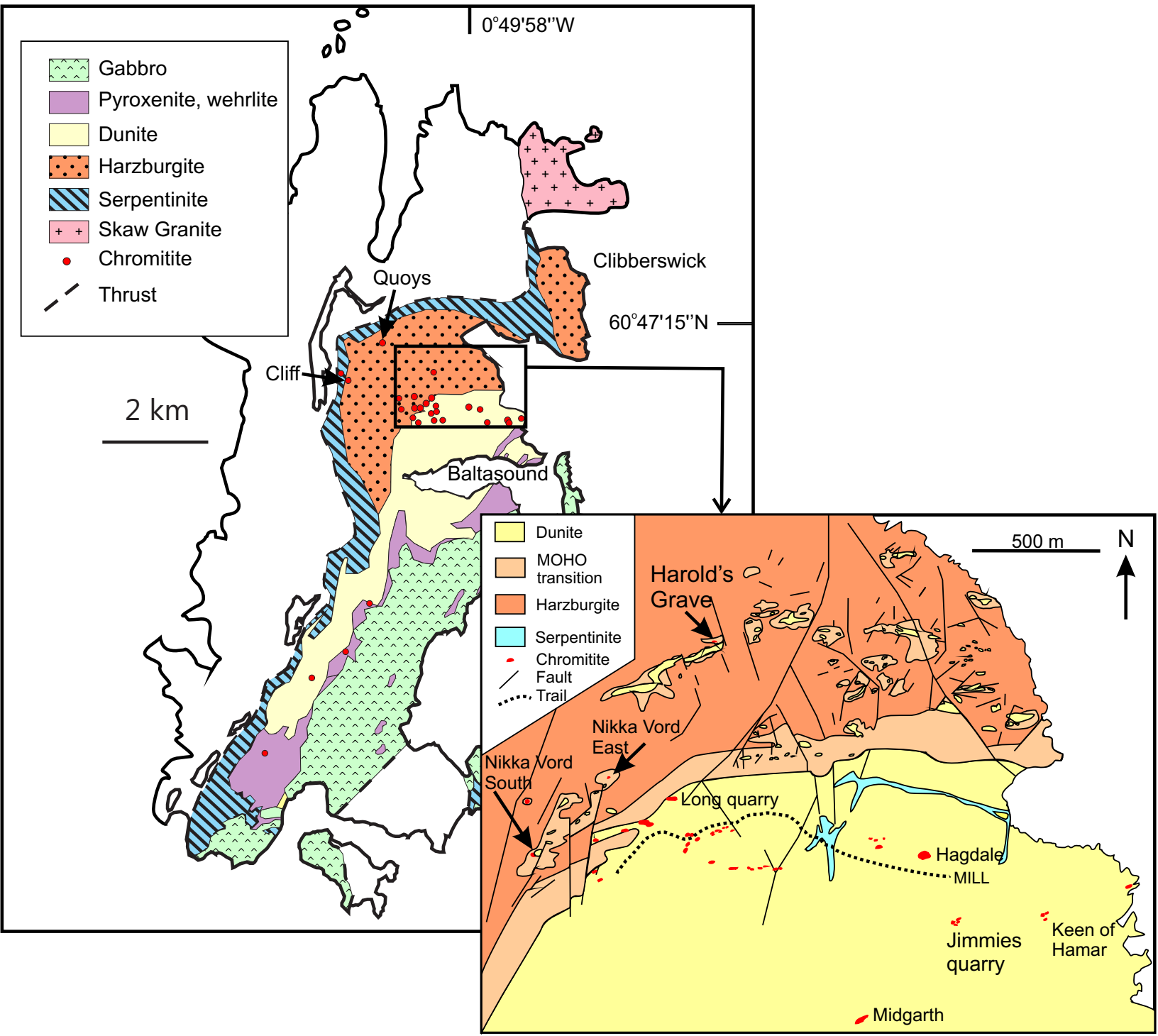
0°49'58''W
60°47'15''N
Gabbro
Pyroxenite, wehrlite
Dunite
Harzburgite
Serpentinite
Skaw Granite
Chromitite
Thrust
Clibberswick
Quoys
Cliff
2 km
Baltasound
Dunite
MOHO transition
Harzburgite
Serpentinite
Chromitite
Fault
Trail
500 m
N
Harold's Grave
Nikka Vord East
Nikka Vord South
Long quarry
Hagdale
MILL
Jimmies quarry
Keen of Hamar
Midgarth

Figure 2

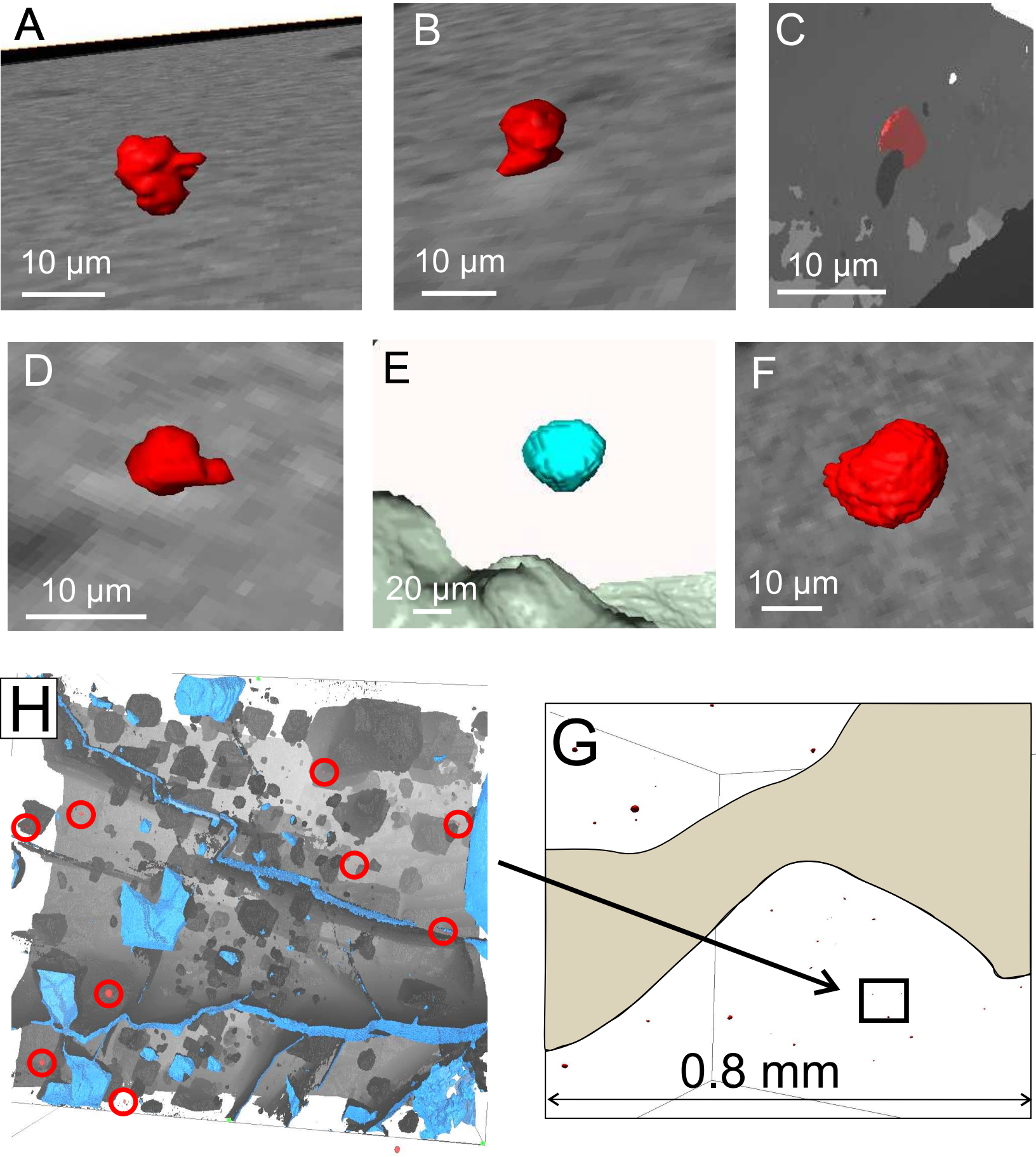

Figure 3

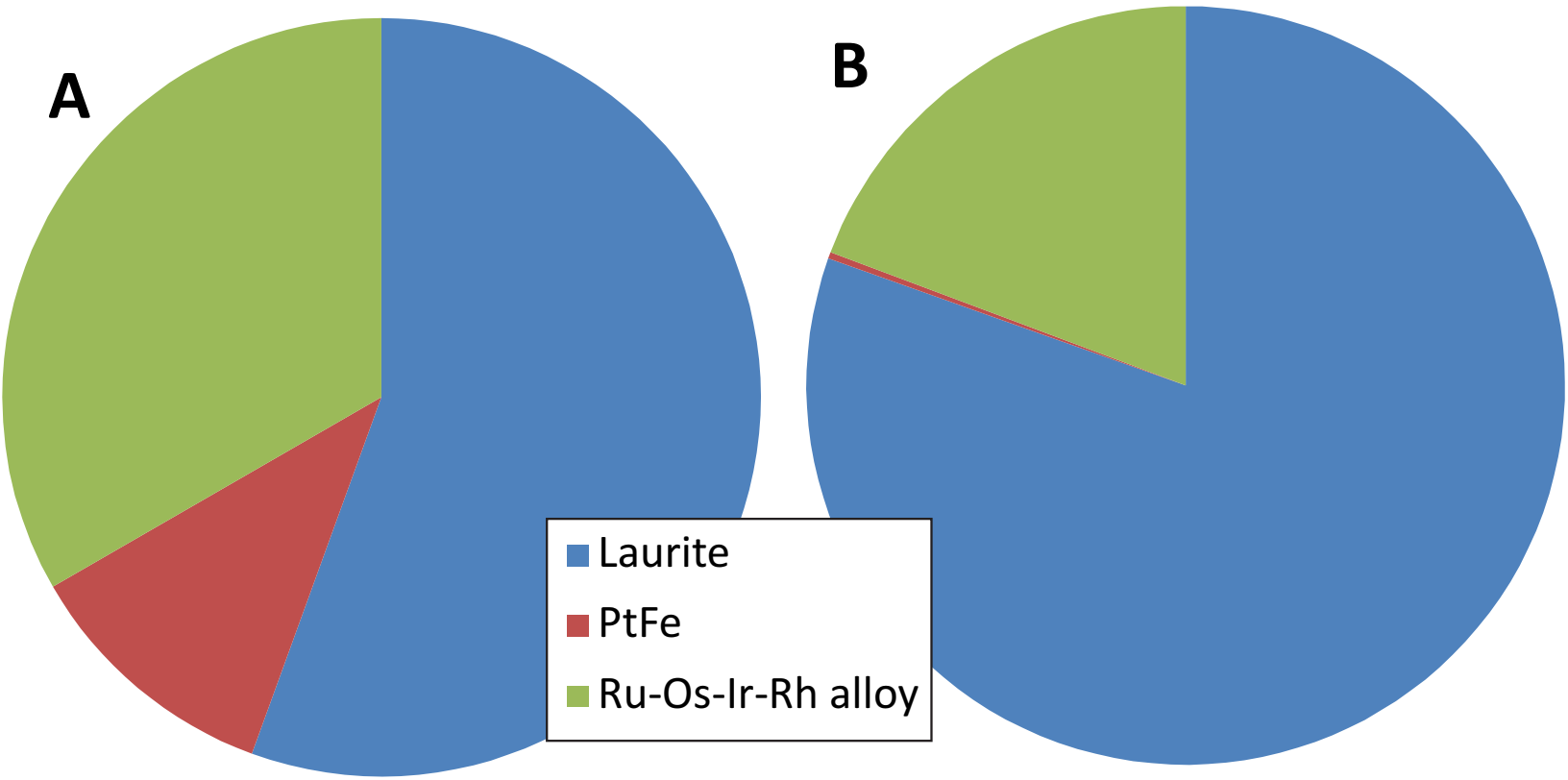

Figure 4

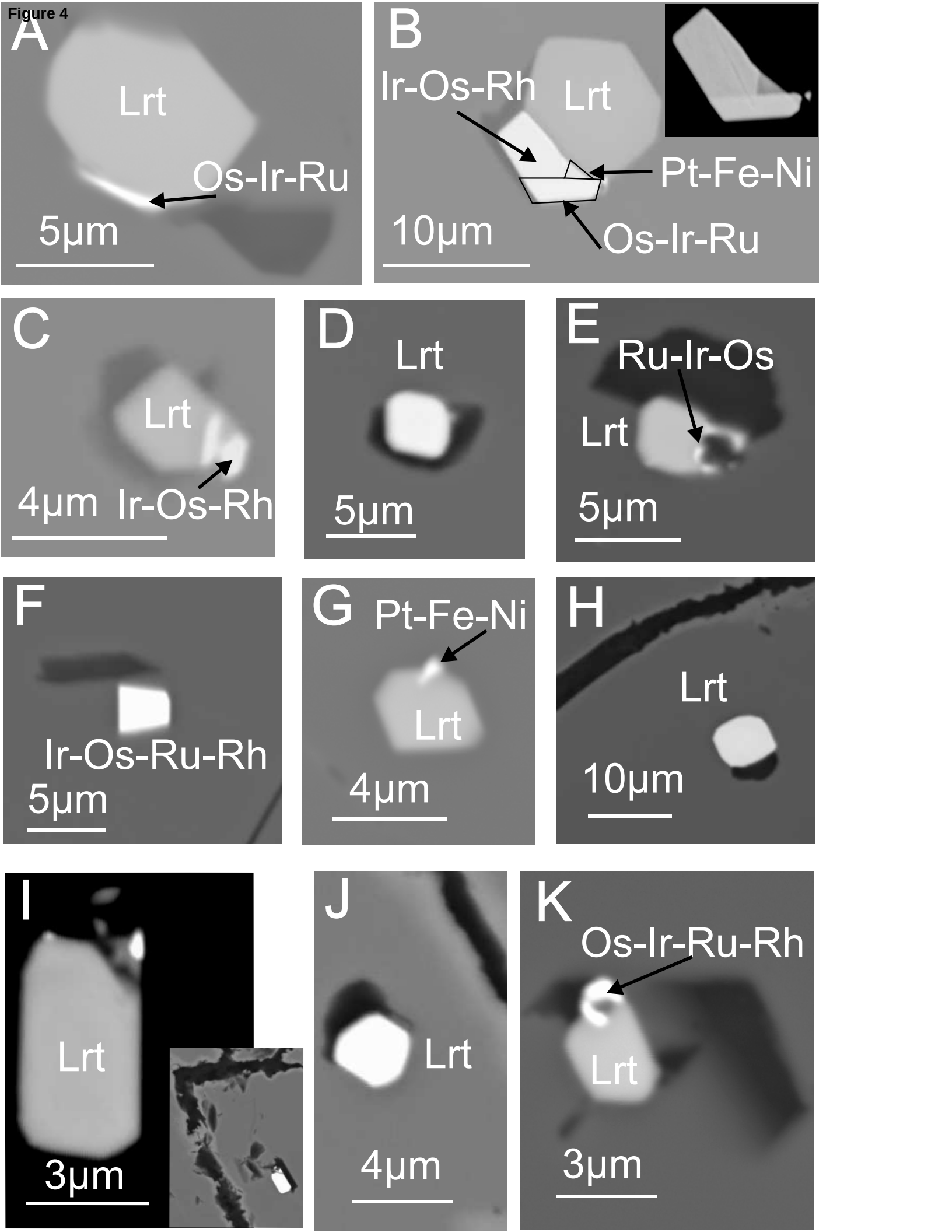
A
Lrt
Os-Ir-Ru
5μm
B
Ir-Os-Rh
Lrt
Pt-Fe-Ni
10μm
Os-Ir-Ru
C
Lrt
4μm
Ir-Os-Rh
D
Lrt
5μm
E
Ru-Ir-Os
Lrt
5μm
F
Ir-Os-Ru-Rh
5μm
G
Pt-Fe-Ni
Lrt
4μm
H
Lrt
10μm
I
Lrt
3μm
J
Lrt
4μm
K
Os-Ir-Ru-Rh
Lrt
3μm

Figure 5

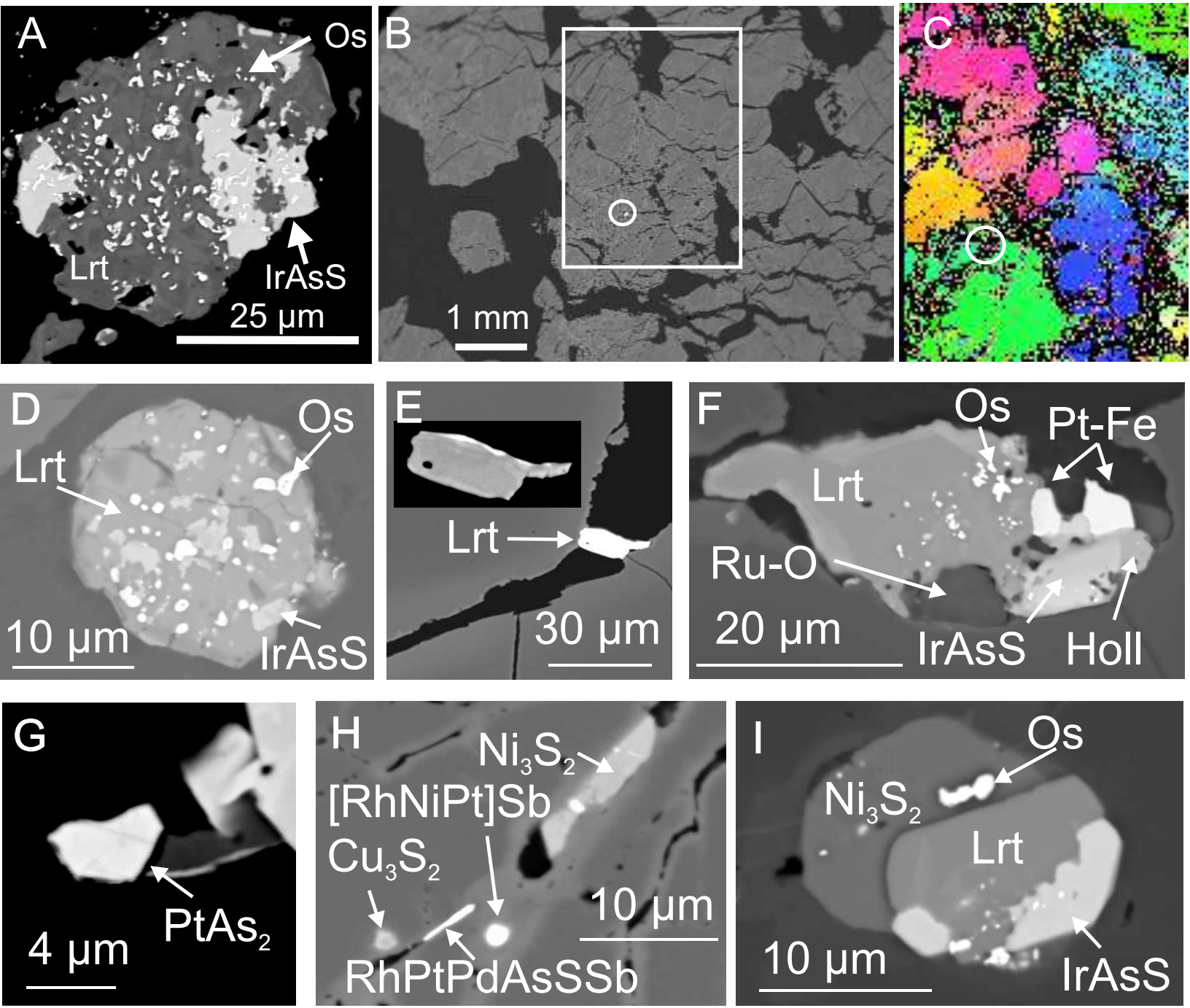
A
Os
Lrt
IrAsS
25 µm
B
1 mm
C
D
Os
Lrt
10 µm
IrAsS
E
Lrt
30 µm
F
Os
Pt-Fe
Lrt
Ru-O
20 µm
IrAsS
Holl
G
PtAs2
4 µm
H
Ni3S2
[RhNiPt]Sb
Cu3S2
10 µm
RhPtPdAsSSb
I
Os
Ni3S2
Lrt
10 µm
IrAsS

Figure 6

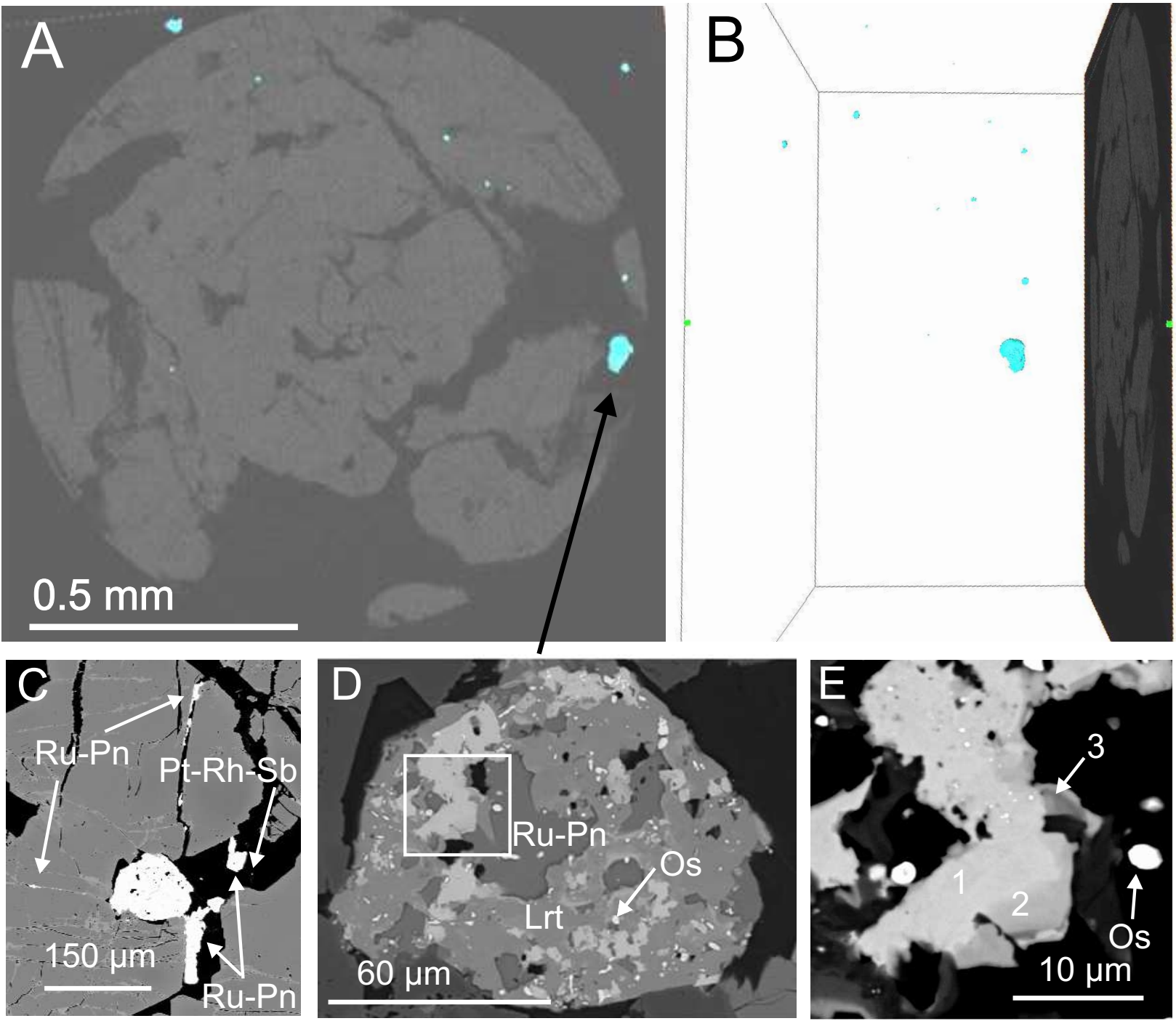
A
0.5 mm
B
C
Ru-Pn
Pt-Rh-Sb
150 μm
Ru-Pn
D
Ru-Pn
Os
Lrt
60 μm
E
3
1
2
Os
10 μm

Figure 7

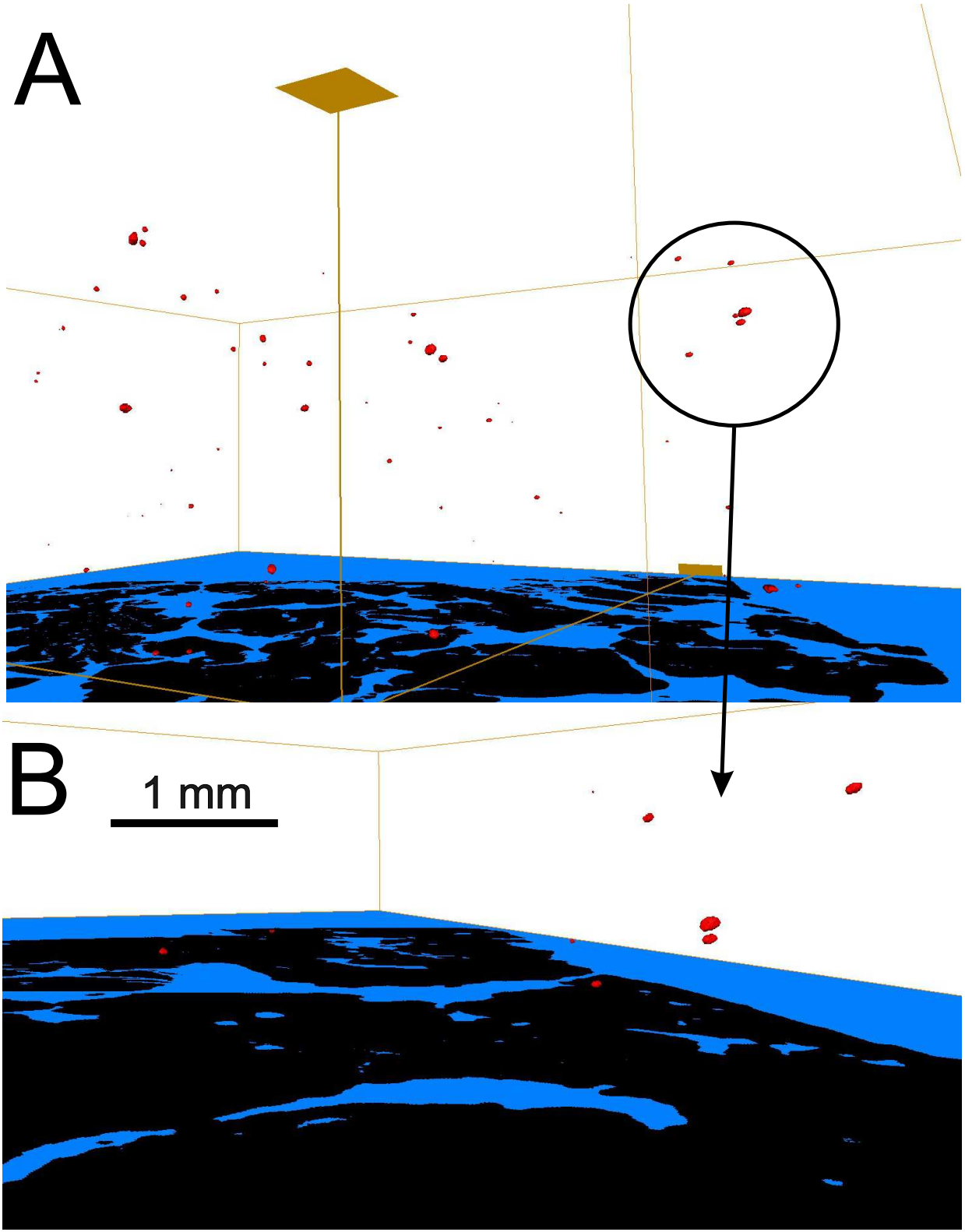

Figure 8

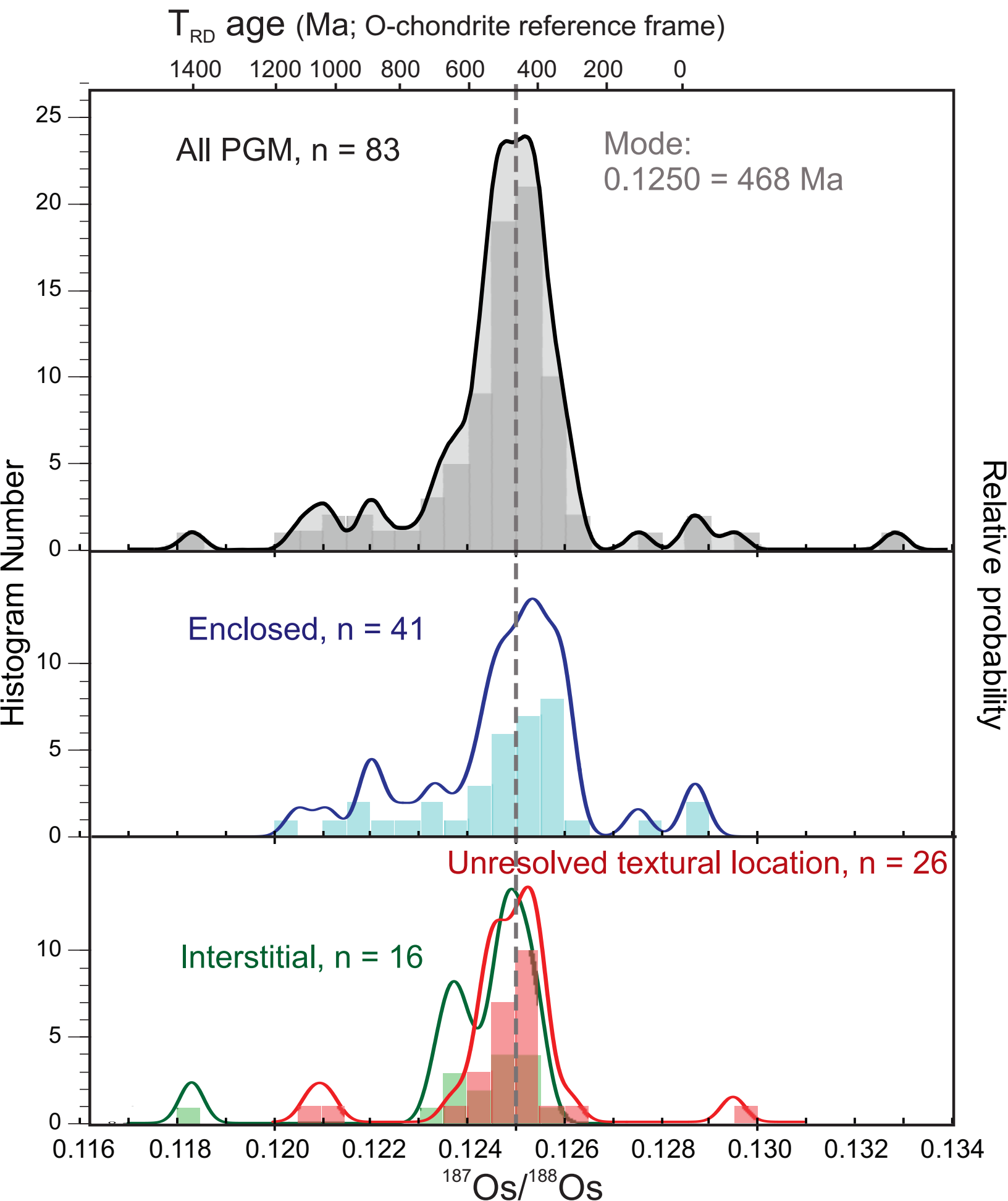
T_RD age (Ma; O-chondrite reference frame)
1400
1200
1000
800
600
400
200
0
All PGM, n = 83
Mode:
0.1250 = 468 Ma
Enclosed, n = 41
Unresolved textural location, n = 26
Interstitial, n = 16
Histogram Number
Relative probability
0
5
10
15
20
25
0.116
0.118
0.120
0.122
0.124
0.126
0.128
0.130
0.132
0.134
187Os/188Os

Figure 9

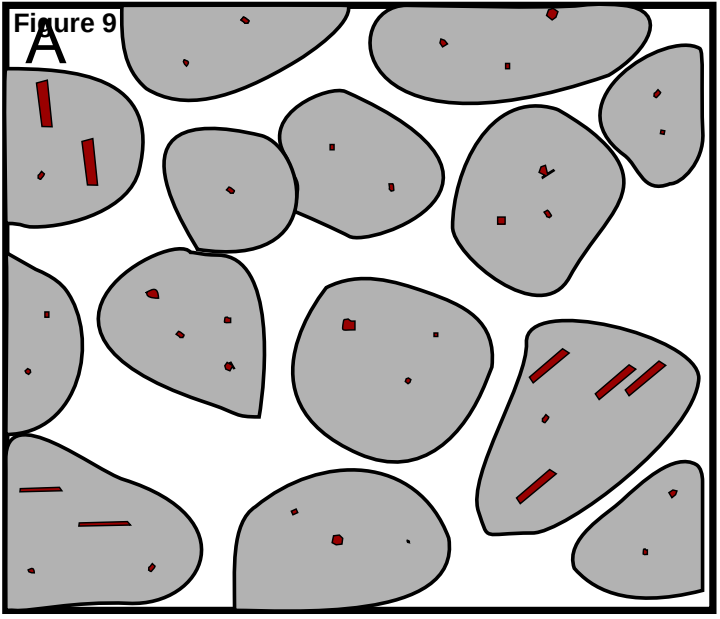


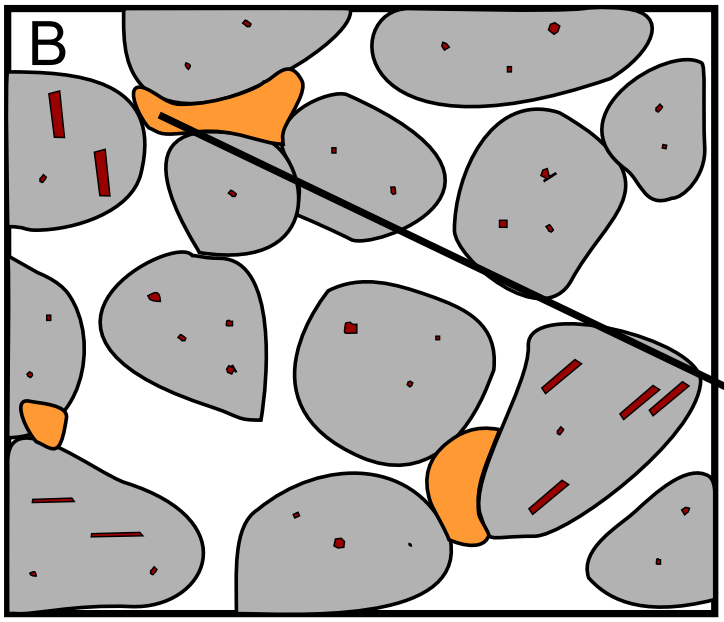


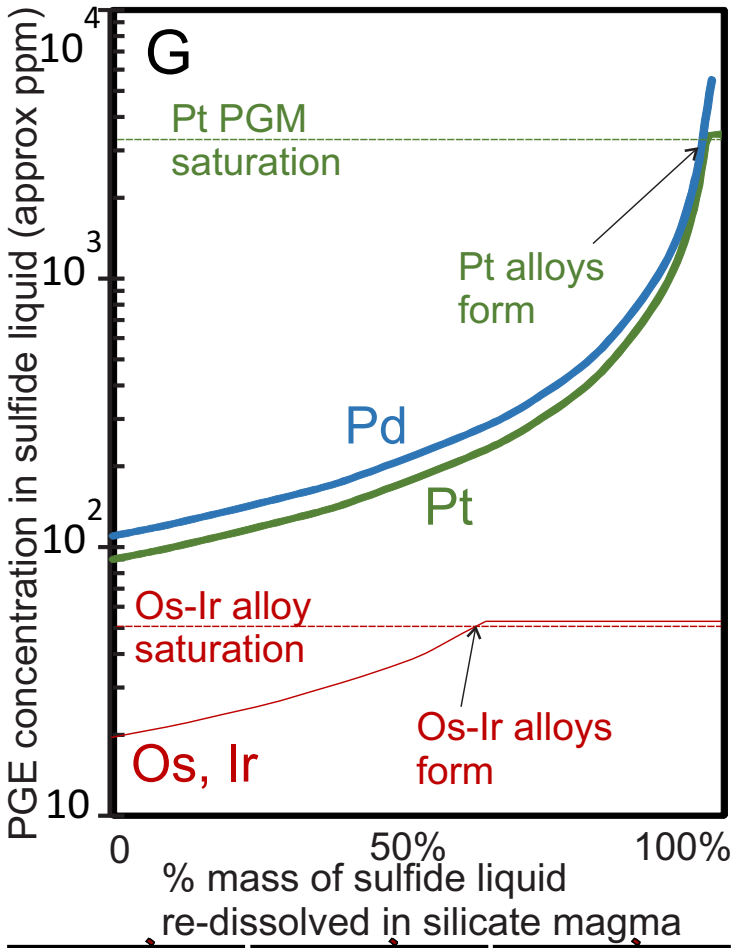


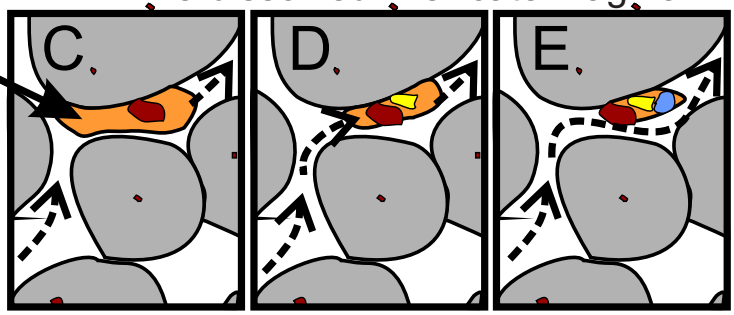


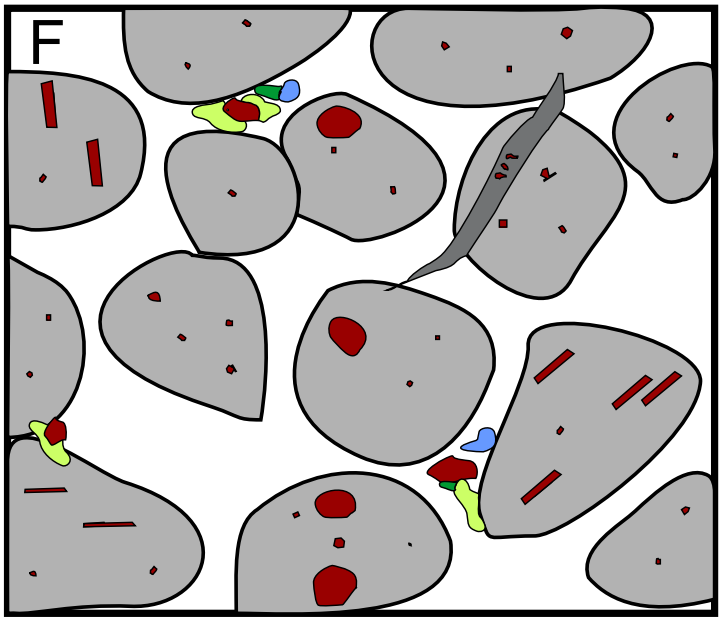


Interstitial serpentine

Chromite grain

PGE-bearing S liquid

Pt-(Pd)-PGM gp (ii)

Ruthenian pentlandite gp (ii)

Irarsite hollingworthite gp (ii)

Os-Ir alloys gp (ii)

Laurite gp (ii)

Laurite with Os-Ir alloys gp (i)

PGM gp (iii)

PGM gp (iv)

PGM gp (v) in shear zone

**Supplementary data table S1**

**Click here to download Electronic Annex: Table Supp S1 HRXCT_table.xlsx**

**Supplementary data table S2**

**Click here to download Electronic Annex: table Supp S2 HG 2016.docx**

**Supplementary data table S3**

**Click here to download Electronic Annex: table Supp S3 HG 2016.docx**

**Supplementary data table S4**

**Click here to download Electronic Annex: Table Supp S4 Os isotopes_CD.xlsx**

**Supplementary figure S1**

Click here to download Electronic Annex: Fig. S1 abundance PGM HG1 6 7.eps

**Supplementary figure S2**

**Click here to download Electronic Annex: Fig. S2 3D big cluster.eps**

**Supplementary figure S3**

**Click here to download Electronic Annex: Fig. S3 HG7 cluster pies.eps**

**Supplementary figure S4**

Click here to download Electronic Annex: Fig. S4 planar array 3D.eps

**Supplementary figure S5**

**Click here to download Electronic Annex: Fig. S5 HHG6a 3D.eps**

**Supplementary figure S6**

**Click here to download Electronic Annex: Fig. S6 lowOs SEM.eps**

**Supplementary figure S7**

**Click here to download Electronic Annex: Fig. S7 SEM notHG.eps**